Electron transport through disordered domain walls: Coherent and incoherent regimes

Peter E. Falloon,[1,2] Rodolfo A. Jalabert,[2,*] Dietmar Weinmann,[2] and Robert L. Stamps[1]
[1]*School of Physics, The University of Western Australia, 35 Stirling Highway, Crawley WA 6009, Australia*
[2]*Institut de Physique et Chimie des Matériaux de Strasbourg, UMR 7504 (CNRS-ULP), 23 Rue du Loess, Boîte Postale 43, 67034 Strasbourg Cedex 2, France*

(Received 17 March 2006; revised manuscript received 30 June 2006; published 25 October 2006)

We study electron transport through a domain wall in a ferromagnetic nanowire subject to spin-dependent scattering. A scattering matrix formalism is developed to address both coherent and incoherent transport properties. The coherent case corresponds to elastic scattering by static defects, which is dominant at low temperatures, while the incoherent case provides a phenomenological description of the inelastic scattering present in real physical systems at room temperature. It is found that disorder scattering increases the amount of spin-mixing of transmitted electrons, reducing the adiabaticity. This leads, in the incoherent case, to a reduction of conductance through the domain wall as compared to a uniformly magnetized region which is similar to the giant magnetoresistance effect. In the coherent case, a reduction of weak localization, together with a suppression of spin-reversing scattering amplitudes, leads to an enhancement of conductance due to the domain wall in the regime of strong disorder. The total effect of a domain wall on the conductance of a nanowire is studied by incorporating the disordered regions on either side of the wall. It is found that spin-dependent scattering in these regions increases the domain wall magnetoconductance as compared to the effect found by considering only the scattering inside the wall. This increase is most dramatic in the narrow wall limit, but remains significant for wide walls.

DOI: 10.1103/PhysRevB.74.144425 PACS number(s): 75.47.Jn, 72.10.−d, 73.23.−b, 75.75.+a

I. INTRODUCTION

The interplay between magnetic structure and electrical resistance in mesoscopic ferromagnetic systems is interesting from both technological and fundamental points of view. Magnetoresistance properties of domain walls represent a particularly striking example of this rich physical problem, and have been intensively studied in recent years. Experiments on ferromagnetic thin films originally found that domain walls contribute to an enhancement of conductance,[1,2] although this was later understood to be due to anisotropic magnetoresistance (AMR) effects.[3] Further experiments on cylindrical Co nanowires[4] and thin polycrystalline Co films[5] have yielded a reduction in conductance, distinct from the positive AMR contribution, which has been attributed to scattering from magnetic domain walls.

From the theoretical side two main approaches exist to address this problem. On one hand, first-principle calculations take into account realistic band structures to study equilibrium properties. Assuming that the resulting one-body wave functions are a good description of the many-body wave functions, a calculational scheme to study electronic transport can be developed. According to the details of the model, large domain wall magnetoresistances may be found.[6,7] On the other hand, phenomenological models including only the essential features of the band structure are extremely useful as they give insight into important physical mechanisms. The most widely used approach is the *sd* model, originally due to Mott,[8] which separates the conduction (s) electrons from those responsible for the magnetic structure (d). The exchange interaction between s and d electrons is incorporated in the spin-splitting Δ of the conduction band. An important advantage of this model is that it can be readily extended to include impurity scattering through a disorder potential, making it particularly suitable for the topic of the present work.

The simplest approach is to treat transport through the domain wall and the leads as ballistic, where the only scattering is due to the rotating spin-dependent potential in the wall. The resulting magnetoconductance is very small for typical domain wall widths,[9,10] although it becomes significant in the special case of domain walls trapped in magnetic nanocontacts.[11–13] In general, the most important effect of a domain wall on ballistic electron transport is a mixing of the up and down spin channels, which arises from the inability of electrons to follow adiabatically the local magnetization direction, referred to as "mistracking."[14,15] When spin-dependent scattering in the regions adjacent to the domain wall is taken into account,[16] this mistracking of spin in a ballistic wall leads to a significant magnetoconductance analogous to the giant magnetoresistance effect.[17]

However, treating the domain wall as a completely ballistic (disorder-free) system is not realistic for experimentally relevant systems. For instance, the cobalt nanowires of Ref. 4 have an estimated elastic mean free path of $\sim$7 nm, while the wall width in cobalt is $\sim$15 nm. Since these two characteristic length scales are of the same order, the transport through the domain wall cannot be described as either ballistic or diffusive. For other materials, such as iron or nickel, the wall widths are larger and, depending on the amount of disorder, the diffusive regime may be reached.

A number of works have focused on the role of disorder scattering inside the domain wall. Viret *et al.*[14] used the ballistic mistracking of spin mentioned above to develop an intuitive picture based on a weighted average of up and down resistances. The estimated relative magnetoresistance decreases with the width of the domain wall and agrees with measurements on domain wall arrays in thin films. Similar results were found using models based on the Boltzmann

equation[18] and the Kubo formula.[19] Phase coherence effects have also been studied,[20,21] and in the case of spin-independent disorder a negative contribution to domain wall magnetoconductance has been predicted.[20,22]

In this work we develop a model for transport through a disordered domain wall based on combining scattering matrices for individual impurity scatterers, which improves on existing treatments in several key aspects. First, the model is nonperturbative in wall width and disorder strength, which allows us to study walls of arbitrary width and consider both ballistic and diffusive transport regimes. It is found that impurity scattering inside the domain wall causes an increase in transmission and reflection with spin-mistracking, or equivalently a reduction in the adiabaticity of spin transport through the wall. Second, we can treat both phase-coherent and incoherent transport regimes within the same model. This permits a quantitative determination of the contribution of phase coherence effects to domain wall magnetoconductance. In this way we find that for incoherent transport a domain wall gives rise to a positive magnetoconductance effect (i.e., a reduction of conductance), which depends on the relative impurity scattering strength for up and down electrons and scales linearly with the number of conductance channels. In constrast, for coherent transport in the case of strong disorder, the domain wall magnetoconductance is negative and does not depend on the relative up/down scattering strength or the system size. Finally, spin-dependent scattering in the regions adjacent to the domain wall can be incorporated directly into the model, allowing us to calculate the total magnetoconductance effect of a domain wall in a nanowire using an approach similar to the circuit model developed in Ref. 16. It is found that scattering in the uniformly magnetized regions on either side of the wall causes an enhancement of the magnetoconductance effect which is largest for narrow walls but is also significant in the wide wall limit.

The layout of this paper is as follows. In Sec. II we introduce our physical model and describe the numerical method which we use to calculate conductance through a disordered region. In Sec. III we study the intrinsic transport properties of a disordered domain wall in both coherent and incoherent regimes. In Sec. IV we incorporate spin-dependent scattering in the regions adjacent to the wall. Finally, in Sec. V we discuss the experimental relevance of our findings, presenting our conclusions and outlook.

II. PHYSICAL MODEL

We consider a quasi-one-dimensional (quasi-1D) wire with the longitudinal axis lying along the z axis and a single transverse dimension of length L_y (see Fig. 1). The position $\vec{r}$ denotes the two-dimensional vector (y,z). The extension to a two-dimensional cross section is straightforward, but complicates the notation and numerical calculations without adding new physics. Within the *sd* model, the conduction electrons in the wire are described by a free-electron one-body Hamiltonian with spin-dependent potential

$$H = -\frac{\hbar^2}{2m}\nabla^2 + \frac{\Delta}{2}\vec{f}(\vec{r})\cdot\vec{\sigma} + V(\vec{r}). \tag{1}$$

Here $\vec{f}(\vec{r})$ is a unit vector in the direction of the effective field representing the magnetic moment due to the d electrons, $\vec{\sigma}$ is the Pauli spin operator of the s electrons, and Δ is the spin-split energy gap between up and down s electrons. The potential $V(\vec{r})$ represents impurities and leads to scattering. It is discussed in detail in Sec. II C.

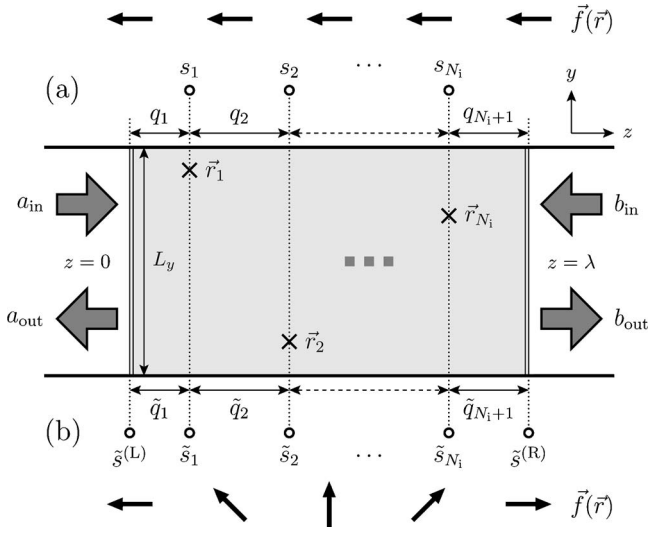

FIG. 1. Schematic illustration of the scattering processes occurring in our model of a disordered wire with (a) uniform magnetization and (b) a domain wall. Above and below the wire are arrows indicating the magnetization direction, $\vec{f}(\vec{r})$, as well as the scattering matrices describing the transport through the wire in each case. The impurities are represented by point scatterers randomly located at $\vec{r}_\alpha$ $(\alpha=1,\ldots,N_i)$, with corresponding scattering matrices s_α (uniform) and $\tilde{s}_\alpha$ (domain wall). The matrices q_α and $\tilde{q}_\alpha$ represent the ballistic propagation between successive scatterers, while $\tilde{s}^{(L,R)}$ represent the scattering from the domain wall interfaces [case (b) only]. These matrices can be combined in a coherent or incoherent way to give the total scattering matrix for the system [Eqs. (12) and (13), respectively]. The incident and scattered fluxes, a_{in}, b_{in} and a_{out}, b_{out}, are also shown.

For a wire uniformly magnetized in the z direction we have $\vec{f}(\vec{r})=(0,0,-1)$ for all $\vec{r}$. When the wire contains a domain wall separating regions of opposite magnetization along the z axis, we have $\vec{f}(\vec{r})=(0,0,-1)$ for $z<0$ and $\vec{f}(\vec{r})=(0,0,1)$ for $z>\lambda$, with the length λ defining the wall region $0\leqslant z\leqslant\lambda$.

For simplicity we assume a square well potential with infinite walls at $y=0,L_y$ for the transverse confinement. In the disorder-free regions of constant magnetization at either end of the system (i.e., the leads), electrons then occupy well-defined modes (channels):

$$\phi_n(y) = \sqrt{\frac{2}{L_y}}\sin\left(\frac{n\pi y}{L_y}\right), \tag{2}$$

where n is a positive integer.

The eigenstates in the leads (which constitute the asymptotic states in a scattering approach to the domain wall) are characterized by a longitudinal wave vector k, transverse mode number n, and spin eigenvalue $\sigma=\pm$ [representing spin states which are, respectively, antiparallel and

parallel to the local direction of $\vec{f}(\vec{r})$]. The corresponding dispersion relation is

$$E = \frac{\hbar^2 k^2}{2m} + \frac{\hbar^2}{2m}\left(\frac{n\pi}{L_y}\right)^2 - \frac{\sigma\Delta}{2}. \tag{3}$$

The relevant states for transport are those with energy E at the Fermi energy E_F, and corresponding wave vectors

$$k_{\sigma n} = \sqrt{k_{\sigma,F}^2 - \left(\frac{n\pi}{L_y}\right)^2}. \tag{4}$$

Here $k_{\sigma,F}=\sqrt{k_F^2+\sigma k_\Delta^2/2}$ is the spin-dependent Fermi wave vector, defined in terms of $k_F=\sqrt{2mE_F/\hbar^2}$ and $k_\Delta = \sqrt{2m\Delta/\hbar^2}$. The number of propagating modes in each lead and for each spin subband, N_σ, is given by the largest value of n for which $k_{\sigma n}$ is real ($N_\sigma \simeq k_{\sigma,F}L_y/\pi$).

These eigenstates can be projected over a position basis, yielding:

$$\langle \vec{r}|\tilde{\psi}_{\sigma n}^{\gtrless}\rangle = \sqrt{\frac{\hbar}{m v_{\sigma n}}} e^{\pm i k_{\sigma n} z} \phi_n(y)|\sigma\rangle, \tag{5}$$

where $\gtrless$ denotes propagation to the right/left, and the spinor basis states $|\pm\rangle$ represent spin eigenstates parallel or antiparallel to the local value of $\vec{f}(\vec{r})$. The states are normalized to unit flux, where the velocity factor for a plane-wave state is $v_{\sigma n}=\hbar k_{\sigma n}/m$.

Defining the spin states $|\sigma\rangle$ with respect to the local magnetization direction allows us to treat both of the leads (as well as the uniform case) within the same notation. Inside the wall ($0 \leqslant z \leqslant \lambda$), $|\sigma\rangle$ depend on $\vec{r}$, and hence the relevant electron eigenstates are more complicated than the states in Eq. (5). They are described in Sec. II B.

The parameters E_F and Δ characterize the structure of the parabolic s band in the sd model, and must be estimated to approximate the spin polarization obtained from realistic band structure calculations. This approximation introduces considerable uncertainty, and we therefore consider a broad range of parameter values in order to understand the possible types of behavior. The situation is simplified considerably by the fact that, in our model, the dependence on the individual parameters E_F, Δ, and λ can be encapsulated in a dimensionless "effective" wall width p_F [Eq. (19b)]. We therefore fix E_F and Δ and explore the different possible physical regimes by varying λ. For definiteness, we choose values for E_F and Δ which may be considered reasonable for Co. Band structure calculations[23,24] find that $E_F \simeq 10$ eV while the splitting between up and down bands is approximately 1 eV. However, the parameter Δ in our model refers to the splitting of the s band, which may be considerably weaker than that of the d band. We therefore take $\Delta=0.1$ eV in this work, while emphasizing that this is a highly uncertain quantity in our model.

A. Scattering matrix approach to conductance

Since we assume noninteracting electrons, the conductance g (in units of e^2/h) may be described by the Landauer-Büttiker formula:[25]

$$g = \sum_{\sigma',\sigma=\pm} \left\{ \sum_{n'=1}^{N_{\sigma'}} \sum_{n=1}^{N_\sigma} T_{\sigma' n';\sigma n}(E_F) \right\}, \tag{6}$$

where $T_{\sigma' n';\sigma n}(E_F)$ is the probability of an electron at energy E_F to be transmitted from the state with spin and transverse mode (σ,n) in the left lead to the one with (σ',n') in the right lead. The use of the sd model is crucial in this approach since the treatment of s and d electrons on the same footing would prevent us from using Eq. (6).

To calculate the transmission amplitudes and probabilities, we use an approach based on combining the scattering matrices of all the scatterers in the system, which was developed to treat transport in spin-independent disordered systems by Cahay *et al.*[26]

Our composition of scattering matrices neglects the effect of evanescent modes, which have an imaginary wave vector and are assumed to decay between successive scattering events. This approximation has been widely used in the so-called local approach for the random matrix description of quasi-1D wires.[27–29] The impressive success of random matrix theory in explaining the universal features of quantum transport, as well as its agreement with numerical simulations and microscopic theories, relies on the hypothesis of a quasi-1D geometry ($L_z \gg L_y$) and weak scattering ($l \gg \delta L \gg k_F^{-1}$, where δL is the size of the scattering blocks). In our case these two hypotheses are valid, since the mean distance between scatterers is much larger than the Fermi wavelength.

For the problem of spin-dependent transport our method offers several important advantages over the spin-dependent extension of the recursive Green's function (RGF) technique. The latter calculates the phase-coherent conductance with a tight-binding approximation for Eq. (1) in which the rotating magnetization and the impurity potential are incorporated through spin-dependent on-site potential energies.[15,30] In particular, the scattering matrix approach allows the conductance to be calculated either coherently or incoherently, which is useful for identifying and understanding phenomena arising from phase coherence. Additionally, because scattering matrices are expressed in terms of local basis states, we are able to avoid the coarse-grained discretization inherent in the tight-binding description of the domain wall magnetization. Finally, because only propagating states are included in the scattering matrices, the computational effort required for a system with a given number of conducting channels is significantly lower than with the RGF technique. In the case of coherent transport through a disordered domain wall, we have verified that results using the scattering matrix approach are in quantitative agreement with those obtained using the RGF technique.[48]

The scattering matrix of a system relates incoming (a_{in},b_{in}) and outgoing (a_{out},b_{out}) flux amplitudes from the left and right (Fig. 1) through

$$\begin{pmatrix} b_{out} \\ a_{out} \end{pmatrix} = s \begin{pmatrix} a_{in} \\ b_{in} \end{pmatrix} = \begin{pmatrix} t & r' \\ r & t' \end{pmatrix} \begin{pmatrix} a_{in} \\ b_{in} \end{pmatrix}. \tag{7}$$

Here t,r (t',r') are transmission and reflection matrices for states incident from the left (right). The elements of these

submatrices are the scattering amplitudes between individual modes (σ,n) and (σ',n'), which we write generically as $\xi_{\sigma' n';\sigma n}$, where ξ stands for one of t, r, t', or r'. The dimension of these submatrices of s is determined by the number of propagating modes of each spin on either side of the scatterer.

Throughout this work we will denote amplitudes and their matrices by lower-case letters and the corresponding probabilities (given by the absolute square of the amplitudes) by upper-case letters. We therefore use s to denote scattering matrices containing amplitudes and S to denote the corresponding matrix of probabilities. This convention differs from the standard notation in which S denotes the scattering matrix of amplitudes, but we adopt it here for notational consistency. The submatrices of S are the transmission and reflection probability matrices T, R, T', and R'. We refer to these matrices generically as Ξ, and the corresponding individual probabilities as $\Xi_{\sigma' n';\sigma n}=|\xi_{\sigma' n';\sigma n}|^2$. We will also make use of the following notation for sums of transmission and reflection probabilities summed over transverse modes and spin:

$$\Xi_{\sigma'\sigma}=\sum_{n'n}\Xi_{\sigma' n';\sigma n}, \tag{8a}$$

$$\Xi_{\sigma}=\sum_{\sigma'}\Xi_{\sigma'\sigma}. \tag{8b}$$

Here $\Xi_{\sigma'\sigma}$ represents the total scattering probability from spin subband σ to σ', and Ξ_{σ} the total scattering probability (into both spin subbands) for states incident with spin σ.

For two scatterers described by the individual scattering matrices s_1 and s_2, the resultant scattering matrix obtained by combining them in series is written as $s_{12}=s_1*s_2$, where the $*$ stands for the composition law

$$t_{12}=t_2(\mathbf{1}-r_1'r_2)^{-1}t_1, \tag{9a}$$

$$r_{12}=r_1+t_1'r_2(\mathbf{1}-r_1'r_2)^{-1}t_1, \tag{9b}$$

$$t_{12}'=t_1'[\mathbf{1}+r_2(\mathbf{1}-r_1'r_2)^{-1}r_1']t_2', \tag{9c}$$

$$r_{12}'=r_2'+t_2(\mathbf{1}-r_1'r_2)^{-1}r_1't_2'. \tag{9d}$$

Here $\mathbf{1}$ denotes the identity matrix with the same number of rows as r_1' and the same number of columns as r_2. The application of this composition law to include many scatterers forms the basis of the approach used in this work.

Coherent and incoherent transport through a disordered region

In this work we are interested in the conductance through a disordered region with either a domain wall or uniform magnetization. As we shall discuss in Sec. II C, the effect of disorder is represented in our model by the potential $V(\vec{r})$, which is comprised of N_i delta function scatterers at randomly distributed positions $\vec{r}_\alpha$. The indices are ordered so that $z_\alpha<z_{\alpha+1}$ for $\alpha=1,\ldots,N_\mathrm{i}$.

Within the scattering matrix approach, the phase-coherent transmission from $z=0$ to λ is calculated by combining the scattering matrices of each delta function scatterer with those for ballistic propagation between the scatterers. We denote these matrices, respectively, by s_α, q_α for uniform magnetization, and $\tilde{s}_\alpha$, $\tilde{q}_\alpha$ for a domain wall. In the case of a domain wall, we also require scattering matrices $\tilde{s}^{(\mathrm{L,R})}$ to describe the scattering at the interfaces between the domain wall and uniform regions. These matrices, and the basis states inside the domain wall, are discussed in detail in the next subsection and in Appendix A.

The matrices q_α and $\tilde{q}_\alpha$ contain the phase shifts acquired by electrons propagating ballistically between scatterers at $\vec{r}_{\alpha-1}$ and $\vec{r}_\alpha$. We write the longitudinal propagation distances as $\delta z_\alpha=z_\alpha-z_{\alpha-1}$, where $z_1,\ldots z_{N_\mathrm{i}}$ are the longitudinal components of the impurity positions and we define $z_0=0$, $z_{N_\mathrm{i}+1}=\lambda$. For the uniform case we have

$$q_\alpha=\begin{pmatrix}\varphi_\alpha & \mathbf{0}\\ \mathbf{0} & \varphi_\alpha\end{pmatrix}, \tag{10}$$

where

$$[\varphi_\alpha]_{\sigma' n';\sigma n}=\delta_{\sigma'\sigma}\delta_{n'n}\exp(ik_{\sigma n}\delta z_\alpha). \tag{11}$$

The matrices $\tilde{q}_\alpha$ for the domain wall case are defined in exactly the same way within the basis of domain wall functions [defined in Eq. (17)], with the domain wall wave vectors $\tilde{k}_{\sigma n}$ [Eq. (18a)] in place of $k_{\sigma n}$.

The total scattering matrices for coherent propagation through the disordered region in the case of a domain wall and uniform magnetization can be written, respectively, as

$$s_{\mathrm{co}}^{(\mathrm{dw})}=\tilde{s}^{(\mathrm{L})}*\tilde{q}_1*\tilde{s}_1*\tilde{q}_2*\cdots*\tilde{s}_{N_\mathrm{i}}*\tilde{q}_{N_\mathrm{i}+1}*\tilde{s}^{(\mathrm{R})}, \tag{12a}$$

$$s_{\mathrm{co}}^{(\mathrm{uni})}=q_1*s_1*q_2*\cdots*s_{N_\mathrm{i}}*q_{N_\mathrm{i}+1}. \tag{12b}$$

For the incoherent conductance, the phase coherence between successive scattering events is assumed to be lost. The resulting scattering matrices for the domain wall and uniform cases are obtained from the combination law of Eq. (9), but using probabilities (Ξ) instead of amplitudes (ξ). We then write

$$S_{\mathrm{inc}}^{(\mathrm{dw})}=\tilde{S}^{(\mathrm{L})}*\tilde{S}_1*\tilde{S}_2*\cdots*\tilde{S}_{N_\mathrm{i}}*\tilde{S}^{(\mathrm{R})}, \tag{13a}$$

$$S_{\mathrm{inc}}^{(\mathrm{uni})}=S_1*S_2*\cdots*S_{N_\mathrm{i}}. \tag{13b}$$

The matrices q_α and $\tilde{q}_\alpha$ do not appear in this case since they contain a pure phase shift and the associated transmission probabilities are simply unity.

In the quasiballistic regime, the elastic mean free path is much larger than the system size and only first-order scattering processes are important. For the uniformly magnetized case the incoherent and coherent conductances become equal in this regime. In the diffusive regime, on the other hand, constructive interference of time-reversed paths with identical starting and end points leads to an enhancement of the coherent reflection known as weak localization.[31] In the limit of large disorder, the coherent conductance enters the strongly localized regime, where g decreases exponentially

with length and the system becomes insulating.[32] By constrast, the incoherent conductance scales like the classical Drude conductance ($g \sim 1/L$), even for arbitrarily large disorder.

A characteristic feature of phase coherence effects in the diffusive regime (such as weak localization or conductance fluctuations) is their universality, or independence of system size, which means that their relative importance is largest for small system sizes. In our model this is particularly significant since we are constrained to work with system sizes that are smaller than typical systems on which experiments are performed. Therefore the relative importance of coherence effects appears overemphasized. On the other hand, the incoherent conductance scales with the system size and our numerical results can be safely extrapolated to larger sizes. Furthermore, in the incoherent case the fluctuations of conductance decrease with increasing disorder, which allows average quantities to be computed accurately with relatively small numbers of samples.

A fundamental limitation with finite numerical models of coherent transport is that, for a given width L_y and impurity density, there is a maximum value of the system length L_z beyond which the system enters the strongly localized regime. However, if L_z is larger than the phase coherence length L_ϕ then the localized behavior obtained in the coherent model is not relevant. A comparison between coherent and incoherent results permits us to determine those features which are due to coherence and which will disappear with increasing temperature. At nonzero temperature the presence of phase-breaking scattering means that the relevant regime for transport is intermediate between the coherent and incoherent limits. It is in general very difficult to treat this regime, but by considering both coherent and incoherent limits we are able to gain some insight into the behavior of experimentally relevant cases.

B. Electronic states in a ballistic domain wall

For our model of a domain wall we assume a linear rotation of $\vec{f}(\vec{r}) \equiv \vec{f}(z)$ in the yz plane over the region $0 \leqslant z \leqslant \lambda$, described by

$$\vec{f}(z) = \begin{cases} (0, \sin[\theta(z)], -\cos[\theta(z)]), & 0 \leqslant z \leqslant \lambda, \\ (0,0,\mathrm{sgn}[z]), & \text{otherwise}, \end{cases} \tag{14}$$

where $\theta(z) = \pi z/\lambda$ is the angle between the magnetization inside the wall and the z axis. Using this profile, one can describe the qualitative features of transport through a domain wall, which have been shown to be independent of the detailed form of the wall.[15] In addition, the profile of Eq. (14) has the advantage that the corresponding basis states can be found in closed form.[15,19] The local spin eigenstates $|\pm\rangle$ [parallel and antiparallel to the direction of $\vec{f}(z)$] are position-dependent inside the domain wall. Denoting the spin basis states with respect to the fixed z axis as $|\pm\rangle_z$, we have

$$|\sigma\rangle = R[\theta(z)]|\sigma\rangle_z, \tag{15}$$

where

$$R[\theta(z)] = \begin{pmatrix} \cos[\theta(z)/2] & -\mathrm{i}\sin[\theta(z)/2] \\ -\mathrm{i}\sin[\theta(z)/2] & \cos[\theta(z)/2] \end{pmatrix} \tag{16}$$

is the spinor rotation operator containing the amplitudes $\langle\sigma'|\sigma\rangle_z$ representing the transformation from fixed to local basis. Because the states $|\pm\rangle$ are position-dependent inside the wall, the eigenfunctions of Eq. (1) in this region are not spin eigenstates, but a combination of both up and down components that projects over a position basis as:

$$\langle \vec{r}|\tilde{\psi}^{\gtrless}_{\sigma n}\rangle = \sqrt{\frac{\hbar}{m\tilde{v}_{\sigma n}}} e^{\pm i\tilde{k}_{\sigma n} z} \phi_n(y)(|\sigma\rangle \pm iA_{\sigma n}|-\sigma\rangle). \tag{17}$$

Here the symbols $\gtrless$ denote the direction of electron propagation (i.e., right or left), while $\sigma = \pm$ is a quantum number representing the spin of the state $|\psi_{\sigma n}\rangle$ to which $|\tilde{\psi}_{\sigma n}\rangle$ reduces in the limit $\lambda \to \infty$. The other parameters are

$$\tilde{k}_{\sigma n} = \sqrt{k_{0n}^2 + k_\lambda^2 + \frac{\sigma}{2}\sqrt{k_\Delta^4 + 16k_\lambda^2 k_{0n}^2}}, \tag{18a}$$

$$A_{\sigma n} = \sigma \frac{2k_\lambda \tilde{k}_{\sigma n}}{\tilde{k}_{\sigma n}^2 + k_\lambda^2 - k_{-\sigma n}^2}, \tag{18b}$$

$$\tilde{v}_{\sigma n} = \frac{\hbar \tilde{k}_{\sigma n}}{m}\left(1 + A_{\sigma n}^2 - \sigma \frac{2k_\lambda A_{\sigma n}}{\tilde{k}_{\sigma n}}\right), \tag{18c}$$

with $k_{0n} = \sqrt{(k_{+,n}^2 + k_{-,n}^2)/2}$ and $k_\lambda = \pi/2\lambda$. The velocity $\tilde{v}_{\sigma n}$ is defined in the usual way as the longitudinal probability flux[33] corresponding to the state $\tilde{\psi}^{>}_{\sigma n}(\vec{r})$. In calculating this quantity, it is necessary to note that the derivative operator in the local spin basis has a nondiagonal form

$$\frac{\partial}{\partial z} = \begin{pmatrix} \dfrac{\partial}{\partial z} & -k_\lambda \\ k_\lambda & \dfrac{\partial}{\partial z} \end{pmatrix}$$

inside the domain wall. As a result, the relation between the velocity factor $\tilde{v}_{\sigma n}$ and wave vector $\tilde{k}_{\sigma n}$ is more complicated than for the uniform basis states in Eq. (5).

The number of propagating modes per spin quantum number inside the domain wall region, $\tilde{N}_\sigma$, is given by the maximum value of n for which $\tilde{k}_{\sigma n}$ is real-valued. For parameter values of interest we generally have $\tilde{N}_\sigma = N_\sigma$. However, for very small λ the rotating potential can lead to effective band gaps (analogous to those occurring in spin-independent periodic potentials), leading to $\tilde{N}_\sigma < N_\sigma$. An additional complication for small λ is that states with complex $\tilde{k}_{\sigma n}$, which are inconvenient to treat within our scattering matrix approach, may become relevant.[49] In the special cases of a ballistic wall or an abrupt wall ($\lambda = 0$), this phenomenon does not affect the calculation of transmission through the wall. However, for the parameter values used in this work ($E_F = 10$ eV, $\Delta = 0.1$ eV) our method breaks down for wall widths in the range $0 < \lambda \lesssim 0.5$ nm. Fortunately, this represents a very

narrow range of parameter values, and the behavior can be readily inferred by interpolating between the values at $\lambda=0$ and 0.5 nm (which we have done in generating Figs. 9, 11, and 12.

In the domain wall model defined by Eq. (14), electrons incident from the left at $z=0$ or from the right at $z=\lambda$ are scattered due to the change from uniform to rotating magnetization. The scattering matrices for these interfaces, which we write $\tilde{s}^{(\mathrm{L})}$ and $\tilde{s}^{(\mathrm{R})}$, can be calculated using the standard method of matching incident and scattered wave-function components. Since the domain wall potential is uniform in the transverse direction (i.e., has no y dependence), the interface does not mix different transverse modes. We thus have $\xi^{(\mathrm{L,R})}_{\sigma' n';\sigma n}=0$ if $n'\neq n$, for $\xi=t,r,t',r'$. The diagonal amplitudes $\xi^{(\mathrm{L,R})}_{\sigma' n;\sigma n}$ are determined by calculating the appropriate scattering state solutions for states incident on the interface, leading to 4×4 sets of linear equations which we present in Appendix A [Eqs. (A1) and (A2)].

For general parameter values it is most convenient to solve Eqs. (A1) and (A2) numerically. However, simple asymptotic expansions can be found in the limits of wide[34] and narrow[15] walls which provide useful insight. In the experimentally relevant case of small spin-splitting and large λ, a particularly simple solution can be found by expanding to second order in the inverse of the dimensionless parameters

$$p_n = k_\Delta^2/2k_{0n}k_\lambda, \tag{19a}$$

$$p_\mathrm{F} = k_\Delta^2/2k_\mathrm{F}k_\lambda. \tag{19b}$$

These parameters characterize the effective "width" of the domain wall for an electron in transverse channel n (p_n) and for the wire as a whole (p_F). The latter can be expressed as $p_\mathrm{F}=\lambda/R_\mathrm{L}$ with the Larmor precession length[34] $R_\mathrm{L}=\pi E_\mathrm{F}/k_\mathrm{F}\Delta$ ($\approx$20 nm for our choice of parameters) which is related to the distance over which an electron at the Fermi energy travels during one Larmor precession of its spin. For an individual channel n, the adiabatic limit corresponds to $p_n\gg 1$ and is most readily obtained for channels with large n (and hence small k_{0n}). As discussed in Ref. 15, the degree of adiabaticity is in general channel-dependent. Nevertheless, p_F permits a characterization of adiabaticity for all states: for a wide wall we have $p_\mathrm{F}\gg 1$, and hence $p_n\gg 1$ for all channels. Within this assumption we solve Eqs. (A1) and (A2) to $O(1/p_n^2)$ for each n, obtaining

$$\tilde{r}^{(\mathrm{L,R})}_{\sigma' n';\sigma n} = \tilde{r}\,'^{(\mathrm{L,R})}_{\sigma' n';\sigma n} = 0, \tag{20a}$$

$$\tilde{t}^{(\mathrm{L,R})}_{\sigma n';\sigma n} = \tilde{t}\,'^{(\mathrm{L,R})}_{\sigma n';\sigma n} = \delta_{n'n}\left(1-\frac{1}{2p_n^2}\right), \tag{20b}$$

$$\tilde{t}^{(\mathrm{L,R})}_{-\sigma n';\sigma n} = -\tilde{t}\,'^{(\mathrm{L,R})}_{-\sigma n';\sigma n} = \mp\,\delta_{n'n}\frac{i}{p_n}. \tag{20c}$$

Equations (20) show that there is essentially no reflection for electrons incident on the domain wall, but that the main effect of the interfaces is to scatter electrons into a superposition of up and down transmitted channels (conserving the mode number), with amplitude determined by p_n.

In the regime of small splitting, $\Delta\ll E_\mathrm{F}$, the transport properties of the domain wall are determined primarily by the parameter p_F, while the dependence on E_F, Δ, and λ individually can, to a good approximation, be neglected. This is true both for the intrinsic domain wall scattering shown in Eqs. (20) and for the impurity scattering to be discussed below. For large splitting, the dependence on Δ becomes important as the difference in the number of up and down conducting channels, N_+-N_-, becomes significant. In this work, however, we are interested only in the case of weak splitting which is relevant for transition metal ferromagnets.

1. Coherent and incoherent transmission for a ballistic wall

Before introducing disorder in the following section, we now briefly consider the case of a disorder-free ballistic domain wall [$V(\vec{r})=0$], which can be treated by setting $N_\mathrm{i}=0$ in Eq. (12a) (coherent case) or Eq. (13a) (incoherent case). An incoherent ballistic system represents an idealized scenario in which electrons are subject to phase-breaking events which do not affect momentum.[35] As such, it is a useful way to treat the effects of decoherence in mesoscopic transport. In the case of a domain wall, it is important to understand the differences between incoherent and coherent transmission in the ballistic case, as this gives insight into effects which are also relevant for the disordered case.

Within the asymptotic approximation of Eqs. (20), the transmission probabilities for coherent and incoherent ballistic walls are, to $O(1/p_n^2)$, given by

$$T_{-\sigma n';\sigma n} = \begin{cases} \delta_{n'n}\dfrac{4}{p_n^2}\sin^2\left(\dfrac{p_n\pi}{4}\right), & \text{coherent,} \\ \delta_{n'n}\dfrac{2}{p_n^2}, & \text{incoherent,} \end{cases} \tag{21a}$$

$$T_{\sigma n';\sigma n} = \delta_{n'n} - T_{-\sigma n';\sigma n}. \tag{21b}$$

From Eqs. (21) the basic difference between the coherent and incoherent cases is a suppression of the oscillatory component of the spin-dependent transmission in the latter case. This occurs because the oscillations observed in the coherent case arise from the phase interference between up and down wall basis state components comprising the electron scattering state, which is suppressed in the incoherent case. This result implies that the oscillatory torques exerted by a spin-polarized current on a domain wall predicted in Ref. 34 would be suppressed if the transport were incoherent.

In Fig. 2 we show the exact total spin-dependent transmission probabilities T_{++} and T_{-+} [defined in Eq. (8a)] as a function of p_F, for both coherent and incoherent ballistic walls. The agreement with the asymptotic results from Eqs. (21) is shown in the inset; it can be seen that these are accurate for moderate to large p_F values, but for small p_F they diverge significantly. We also note that, although not explicitly shown in Fig. 2, the total reflection from the ballistic domain wall is negligible except near the abrupt limit ($\lambda=0$). In the limit of many channels when $N_+>N_-$, the channel blocking mechanism occurring for an abrupt wall[15]

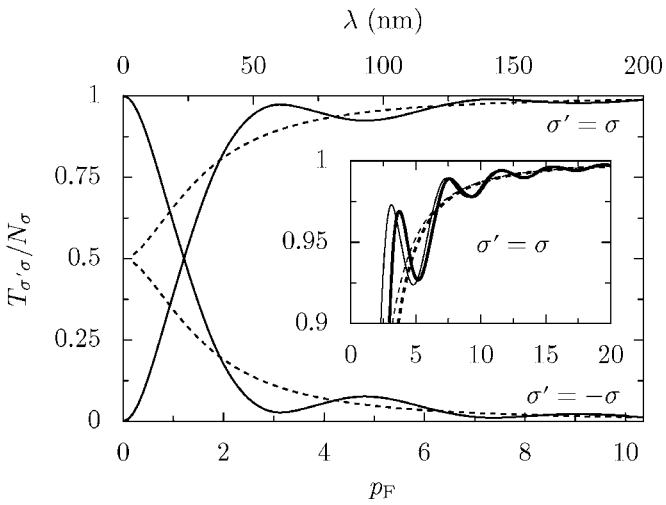

FIG. 2. Spin-dependent transmission per incoming channel, $T_{\sigma'\sigma}/N_\sigma$, for a ballistic domain wall as a function of the dimensionless effective wall width p_F (bottom axis). For comparison, the corresponding actual wall width λ for parameter values $E_F=10$ eV and $\Delta=0.1$ eV is also shown (top axis). The curves presented are for $\sigma=+$, with $\sigma'=\pm\sigma$, and are indistinguishable from the corresponding ones for $\sigma=-$ (for the parameter values used). Solid and dashed lines indicate, respectively, coherent and incoherent combinations of scattering matrices. The actual wire width used is $L_y=5$ nm, corresponding to $N_\pm=25$, but the curves are indistinguishable from their form in the limit of large L_y. Inset: comparison of the asymptotic solutions for $T_{\sigma\sigma}$ from Eq. (21b) (thick lines) with the exact values (thin lines) over a larger range of p_F.

leads to a relative change in conductance of the order of Δ/E_F (~0.01 in this case). However, we have chosen parameters such that $N_+=N_-$. Then, the channel blocking is irrelevant.

In the limit $p_F\to 0$, the exact solutions show that the incoherent transmission goes to $N_\sigma/2$, which is somewhat surprising since we expect complete mistracking [i.e., $T_{\sigma\sigma}=0$] in this limit, as is observed for the coherent case. The origin of this result can be understood as follows. By combining scattering matrices incoherently we are effectively "measuring" the individual path taken by an electron going through the wall, so that is projected onto one of the right-moving wall basis states $|\psi_\pm^>\rangle$. Since each of these states comprises an equal weighting of local up and down components as $p_F\to 0$, the incoherent combination must also yield an equal weighting. It is clear that the incoherent result is unphysical for small p_F, since there will always be some nonzero distance over which transport is coherent. We therefore need to be careful when interpreting the incoherent results for small p_F.

C. Delta function model of scattering

In transition metal ferromagnets the elastic spin-conserving scattering of conduction electrons arises from a variety of mechanisms, including impurities, defects, and grain boundaries. These scattering rates depend on the underlying details of band structure, and are in general strongly spin-dependent. In spite of this complex situation, the strength of elastic scattering can be characterized by only two parameters, namely, the spin-dependent elastic mean free paths $l_\pm$. The precise microscopic model leading to a given value of $l_\pm$ is then of minor importance. In the *sd* model the spin dependence of l_σ arises from two sources:[36] the intrinsic spin dependence of the electron wave vectors $k_{\sigma n}$ and a difference in the number of available *d* states of each spin into which the conducting *s* electrons can be scattered. The former effect is due to the spin-splitting of the *s* band, which makes $k_{+,n}>k_{-,n}$. Therefore electrons with spin up are generally less strongly scattered than those with spin down, which in the absence of other sources of spin dependence leads to $l_+>l_-$. However, since we work in the regime of small splitting, $\Delta\ll E_F$, this difference is rather small. The dominant contribution then comes from scattering into the *d* band. The resulting spin dependence can lead to $l_+>l_-$ or $l_+<l_-$ depending on the form of the up and down *d* subbands at the Fermi energy. For definiteness, we assume that the spin down *d* subband has a greater number of states at E_F than the spin up subband, which implies that spin down electrons are the more strongly scattered ones, leading to $l_+>l_-$. To represent scattering processes, we adopt a simplified picture in which *s* electrons are scattered by the static potential $V(\vec{r})$. The degrees of freedom corresponding to the *d* electrons are therefore not explicitly included and, in particular, we ignore the possibility that electrons scattered into *d* states might not return to the *s* band. However, one might expect that the behavior of the system depends essentially on the spin-dependent mean free paths l_+ and l_-, and that the microscopic details of the model leading to their values are of minor importance.

The potential $V(\vec{r})$ is defined as a random array of delta functions with spin-dependent amplitudes $u_\pm$, where the orientations are defined with respect to the local magnetization direction $\vec{f}(z)$. The delta function model is a convenient phenomenological approach to impurity scattering which has been widely used in spin-independent mesoscopic transport theories[26,37] as well as in ferromagnetic systems.[18,20] The spin dependence of scattering in the ferromagnet is determined by the ratio of up and down amplitudes, which we write as $\rho=u_-/u_+$. For spin-dependent impurity scattering we take $\rho>1$, which corresponds to $l_+>l_-$. For completeness, we will also consider the case of spin-independent impurity scattering, $\rho=1$.

We write the up and down components of $V(\vec{r})$ in the local spin basis as

$$V_\sigma(\vec{r}) = u_\sigma \sum_{\alpha=1}^{N_i} \delta(\vec{r}-\vec{r}_\alpha), \tag{22}$$

where there are N_i impurities with positions $\vec{r}_\alpha$ randomly distributed in a region of area $L_y\times L_z$. In general, L_z may be different from the domain wall length λ. The impurity density is $n_i=N_i/L_yL_z$. The total impurity potential can then be written as a sum of spin-independent and dependent terms:

$$V(\vec{r}) = \frac{V_+(\vec{r})+V_-(\vec{r})}{2}\mathbb{1} + \frac{V_+(\vec{r})-V_-(\vec{r})}{2}\vec{f}(z)\cdot\vec{\sigma}. \tag{23}$$

Alternatively, the potential can be written in a diagonal form

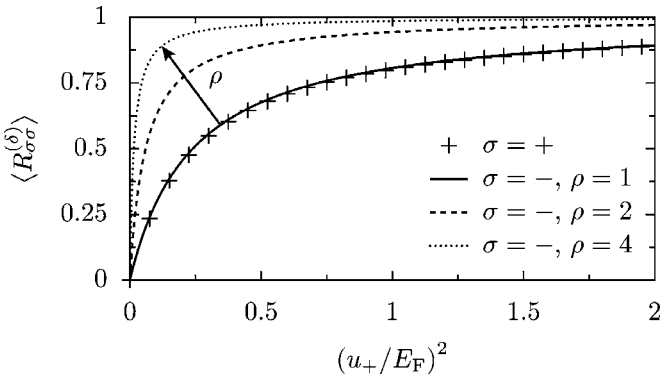

FIG. 3. Total spin-dependent reflection from a delta function scatterer with spin-dependent amplitudes u_σ in the uniformly magnetized case, $\langle R^{(\delta)}_{\sigma\sigma}\rangle$ (averaged over transverse positions y_α). Curves are shown as a function of $(u_+/E_F)^2$ for different values of the up/down scattering ratio $\rho=u_-/u_+$. For $\rho=1$ the only spin dependence of scattering is due to the small difference between $k_{+,n}$ and $k_{-,n}$, and hence $\langle R^{(\delta)}_{--}\rangle \simeq \langle R^{(\delta)}_{++}\rangle$. For small u_σ, $\langle R^{(\delta)}_{\sigma\sigma}\rangle$ goes as u^2_σ [Eq. (C4a)], while for large u_σ it approaches a maximum value of 1. The particular system used in this calculation has $L_y=2$ nm, giving $N_\pm=10$.

$$V(\vec{r}) = R^{-1}[\theta(z)]\begin{pmatrix} V_+(\vec{r}) & 0 \\ 0 & V_-(\vec{r}) \end{pmatrix} R[\theta(z)], \tag{24}$$

in terms of the rotation matrix $R[\theta(z)]$ defined in Eq. (16).

As shown in Eqs. (12) and (13), the transmission through the disorder potential can be calculated by combining the scattering matrices s_α, $\tilde{s}_\alpha$ of the individual delta function scatterers located at $\vec{r}_\alpha$, together with the matrices q_α and $\tilde{q}_\alpha$ for propagation between successive scatterers. The dependence on the longitudinal component of the scatterer position, z_α, is contained in q_α and $\tilde{q}_\alpha$, while the dependence on the transverse component, y_α, is contained in s_α and $\tilde{s}_\alpha$. We therefore write the scattering matrix for a delta function scatterer located at $\vec{r}_\alpha$ as $s^{(\delta)}(y_\alpha)$ (uniform) and $\tilde{s}^{(\delta)}(y_\alpha)$ (domain wall). We describe the calculation of these scattering matrices in Appendix B and present solutions valid in the Born approximation in Appendix C.

To understand the scattering from a delta function with spin-dependent amplitudes u_σ, it is useful to consider the total spin-dependent reflection for the uniform case, $R^{(\delta)}_{\sigma\sigma}$. Figure 3 shows $\langle R^{(\delta)}_{\sigma\sigma}\rangle$, the reflection averaged over transverse positions y_α of the scatterer, as a function of u_σ for several values of ρ. For small u_σ, we see that $\langle R^{(\delta)}_{\sigma\sigma}\rangle$ goes as u^2_σ, which can also be seen directly from the Born approximation.[38] The ratio of up to down backscattering thus goes as ρ^2 for small u_σ. For larger u_σ, however, $\langle R^{(\delta)}_{\sigma\sigma}\rangle$ is bounded above by 1, attaining this value in the limit $u_\sigma \to \infty$. This occurs because a delta function scatterer can "block" at most one channel.[39] The spin dependence of reflection is then dramatically reduced for large u_σ. Since our goal in this work is a model with spin-dependent scattering, we must therefore work in the regime of small u_σ. However, we cannot take u_σ arbitrarily small, since decreasing u_σ means that a larger N_σ is required to achieve a given disorder density, leading to an increase in computation time. In practice we have found $u_+ \lesssim E_F/5$ to be a useful compromise for parameters in the range $1 \leqslant \rho \leqslant 2$.

III. TRANSPORT THROUGH A DISORDERED DOMAIN WALL: INTRINSIC PROPERTIES

In this section we consider the intrinsic conductance properties of a disordered domain wall. Here the domain wall constitutes the entire system of interest, i.e., $L_z=\lambda$, and is therefore assumed to be connected on either side to perfect (disorder-free) leads. By comparing with a uniformly magnetized disordered region of the same length, we calculate an intrinsic domain wall magnetoconductance which measures the difference in conductance due to the presence of a domain wall. We consider both coherent and incoherent regimes; the corresponding scattering matrices for the system are obtained from Eqs. (12) and (13). Our primary aim in this section is to study the role of impurity scattering inside the domain wall. The case of most interest is spin-dependent disorder ($\rho>1$), however, in order to relate our model to previous works and more clearly understand aspects of the spin-dependent case, we also consider spin-independent disorder, $\rho=1$.

In the uniform case, the two spin subbands of conduction electrons are uncoupled, so there is no spin mixing. All off-diagonal (in spin quantum numbers) transmission and reflection amplitudes are therefore zero, i.e., $\xi_{-\sigma n';\sigma n}=0$ for $\xi=t,r,t',r'$. The total spin-dependent transmission and reflection probabilities [defined in Eqs. (8)] satisfy

$$\Xi^{(\mathrm{uni})}_{-\sigma\sigma}=0, \quad \Xi^{(\mathrm{uni})}_{\sigma}=\Xi^{(\mathrm{uni})}_{\sigma\sigma}, \tag{25}$$

for $\Xi=T,R,T',R'$.

The conductance properties of the up and down subbands of the uniform system are well-described by random matrix theory,[27,40] whose expressions for the average transmission and its moments are in excellent quantitative agreement with the calculations performed with our model. For a system of length L_z, the total transmission for spin subband σ in the incoherent case is given by

$$\langle T^{(\mathrm{uni})}_{\sigma,\mathrm{inc}}\rangle = N_\sigma/(1+L_z/l_\sigma), \tag{26}$$

where N_σ is the number of channels and l_σ is the spin-dependent elastic mean free path. Equation (26) expresses the transmission as a series combination of the ballistic contact transmission, N_σ, with the Drude conductance, $N_\sigma l_\sigma/L_z$. In the diffusive regime, $l_\sigma \ll L_z$, the Drude term dominates and $\langle T^{(\mathrm{uni})}_{\sigma,\mathrm{inc}}\rangle$ displays an ohmic $1/L_z$ dependence. In the quasiballistic regime, $l_\sigma \gg L_z$, Eq. (26) is only approximately correct, but is within several percent of the value obtained by a more precise calculation.[41]

For delta function scatterers in a two-dimensional quasi-1D geometry, the mean free path l_σ appearing in Eq. (26) is given by

$$l_\sigma = \frac{2\hbar^3 v_{\sigma,F}}{m n_i u^2_\sigma}, \tag{27}$$

where $v_{\sigma,F}=\hbar k_{\sigma,F}/m$ is the Fermi velocity in spin subband σ. This definition is a factor of 2 larger than the two-

dimensional form[42] since in a quasi-1D geometry forward scattering processes do not reduce transmission.[43]

The mean free path l_σ can be interpreted intuitively as the typical distance traveled by an electron of spin σ before undergoing a momentum randomizing scattering event. However, it should be noted that such a conceptual scattering event does not correspond to the scattering from an individual delta function scatterer in our model: the length l_σ typically corresponds to a large number of individual scatterers.

The coherent transmission, $\langle T^{(\mathrm{uni})}_{\pm,\mathrm{co}}\rangle$, is reduced with respect to $\langle T^{(\mathrm{uni})}_{\pm,\mathrm{inc}}\rangle$ by the weak localization correction, which in a quasi-1D system has the limiting value $-1/3$ in the diffusive regime $L_z/l_\sigma \gg 1$.[27,40]

A. Disorder-induced enhancement of spin-mistracking in domain wall transport coefficients

We first consider how the transport coefficients of a domain wall vary as a function of disorder. It is most instructive to study the total spin-dependent transmission and reflection, summed over all transverse channels and averaged over impurity configurations, $\langle T^{(\mathrm{dw})}_{\sigma'\sigma}\rangle$ and $\langle R^{(\mathrm{dw})}_{\sigma'\sigma}\rangle$. In Fig. 4 these quantities are shown for a relatively wide wall ($p_\mathrm{F}=5$) with spin-dependent disorder ($\rho=2$) as a function of disorder strength ($1/l_+$ in units of $1/\lambda$). Both coherent [Eq. (12a)] and incoherent cases [Eq. (13a)] are shown.

At zero disorder, $1/l_+=0$, transport through the ballistic wall is highly adiabatic, so that $\langle T^{(\mathrm{dw})}_{\sigma\sigma}\rangle \gg \langle T^{(\mathrm{dw})}_{-\sigma\sigma}\rangle$. With increasing disorder, the dominant transmission coefficient, $\langle T^{(\mathrm{dw})}_{\sigma\sigma}\rangle$, decreases quite rapidly, with a form similar to that of the transmission in the uniform case, $\langle T^{(\mathrm{uni})}_{\sigma\sigma}\rangle$ [Eq. (26)]. Also, we observe that $\langle T^{(\mathrm{dw})}_{--}\rangle$ decreases more rapidly than $\langle T^{(\mathrm{dw})}_{++}\rangle$, since $l_-<l_+$. These initial decays can be quantitatively described by the Born approximation of Appendix C, and the coherent and incoherent cases yield very similar results.

The off-diagonal (in spin) coefficients $\langle T^{(\mathrm{dw})}_{-\sigma\sigma}\rangle$ also exhibit a linear decrease with $1/l_+$ in the quasiballistic regime. However, for a relatively weak disorder ($\lambda/l_+\simeq 1$) the behavior of off-diagonal coefficients begins to differ considerably from that of the diagonal ones. As we can see in the inset of the upper graph in Fig. 4, the negative slope of the coherent $\langle T^{(\mathrm{dw})}_{-\sigma\sigma}\rangle$ levels off, and the incoherent $\langle T^{(\mathrm{dw})}_{-\sigma\sigma}\rangle$ increases with disorder.

In both cases (coherent and incoherent), the magnitude of $\langle T^{(\mathrm{dw})}_{-\sigma\sigma}\rangle$ remains relatively constant as a function of disorder. This means that the *relative* transmission with spin-mistracking, $\langle T^{(\mathrm{dw})}_{-\sigma\sigma}\rangle/(\langle T^{(\mathrm{dw})}_{\sigma\sigma}\rangle+\langle T^{(\mathrm{dw})}_{-\sigma\sigma}\rangle)$, increases dramatically as a function of disorder. Furthermore, since $\langle T^{(\mathrm{dw})}_{--}\rangle<\langle T^{(\mathrm{dw})}_{++}\rangle$ while $\langle T^{(\mathrm{dw})}_{+-}\rangle=\langle T^{(\mathrm{dw})}_{-+}\rangle$, the proportion of transmission with mistracking is greater for the spin down than for the spin up subband.

The case of spin-independent disorder, $\rho=1$ (not shown), is qualitatively similar to the spin-dependent case just discussed, with the difference that $\langle T_{++}\rangle\simeq\langle T_{--}\rangle$ and $\langle R_{++}\rangle\simeq\langle R_{--}\rangle$. This is because in this case the only spin dependence of the scattering arises from the small spin dependence of the wave vectors $\tilde{k}_{\sigma n}$.

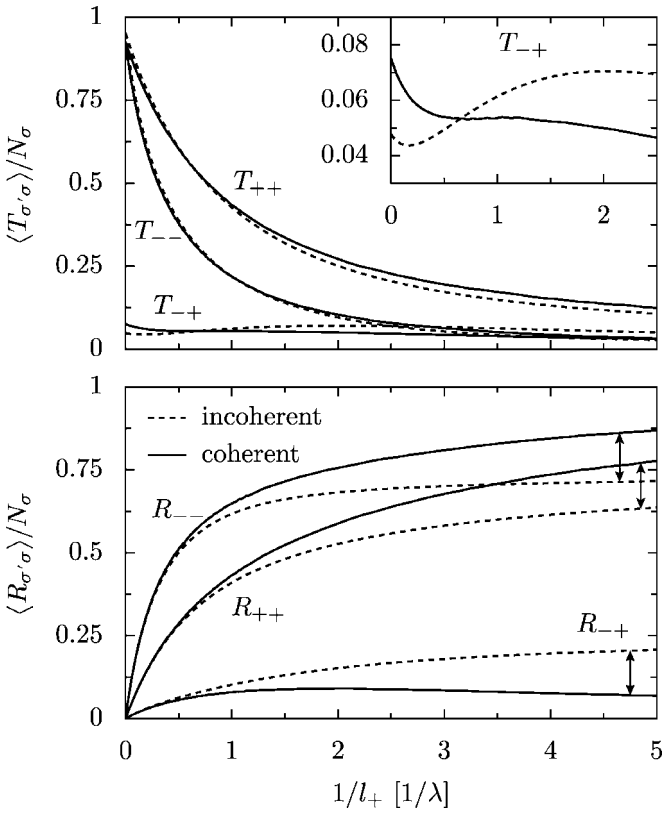

FIG. 4. Spin-dependent domain wall transmission and reflection, $\langle T_{\sigma'\sigma}\rangle$ and $\langle R_{\sigma'\sigma}\rangle$ (normalized by the number of conducting modes per incident spin channel, N_σ), as a function of disorder, measured by $1/l_+$ (shown in units of $1/\lambda$). Coherent (solid lines) and incoherent (dashed lines) cases are shown (the arrows connect corresponding values). The wall width is $p_\mathrm{F}=5$, which corresponds to a wide wall close to the adiabatic limit ($T_{\sigma\sigma}\gg T_{-\sigma\sigma}$ for the ballistic wall at $1/l_+=0$). The parameters for the delta function scatterers are $u_+=E_\mathrm{F}/5$ and $\rho=2$, and the averages are performed using $N_\mathrm{S}=2000$ impurity configurations. The wire width is $L_y=10$ nm, leading to $N_\pm=51$.

The preceding observations imply that the adiabaticity which applies to ballistic domain wall transport no longer applies in the presence of disorder. In particular, *a wall which is highly adiabatic in the regime of ballistic transport becomes less so in the presence of disorder*. For spin-independent disorder, a similar result was recently obtained in the context of transport through disordered wires in the presence of inhomogeneous magnetic fields.[44] For spin-dependent disorder, the reduction in adiabaticity depends on the spin direction, so the wall can no longer be characterized by a single adiabaticity parameter as it was in the ballistic case.[16] The origin of the enhancement of mistracking with increasing disorder can be understood intuitively as the cumulative effect of small amounts of mistracking acquired in scattering from each individual delta function [see Eqs. (C2b) and (C2d)]. We illustrate this important idea with a simple one-dimensional toy model in Appendix D.

Finally, we note several differences between the coherent and incoherent cases in Fig. 4. In the ballistic case, $1/l_+=0$,

there is a small difference between $\langle T^{(\mathrm{dw})}_{\sigma'\sigma,\mathrm{co}}\rangle$ and $\langle T^{(\mathrm{dw})}_{\sigma'\sigma,\mathrm{inc}}\rangle$. This is due to suppression of the oscillatory component of the coherent transmission, which was discussed in Sec. II B 1 and illustrated in Fig. 2. This difference may be positive or negative, depending on p_{F}, and becomes increasingly significant as $p_{\mathrm{F}}\to 0$. The effect persists for small $1/l_+$, but disappears for larger disorder since the phase information corresponding to the precessional component is lost after many scattering events.

A second difference between the coherent and incoherent cases is that for large disorder the scattering coefficients with mistracking, $\langle T^{(\mathrm{dw})}_{-\sigma\sigma}\rangle$ and $\langle R^{(\mathrm{dw})}_{-\sigma\sigma}\rangle$, are smaller for the coherent case than for the incoherent one. The precise origin of this difference is not clear, but we can eliminate several possible reasons. First, by looking at the equivalent curves for different values of p_{F}, it is found that the difference has a constant sign for all λ. This suggests that it cannot be explained by the suppression of the precessional component of transmission in the incoherent case, as invoked in the discussion of the previous paragraph. Furthermore, it is found that the difference scales linearly with the number of channels N_σ (or equivalently L_y). It cannot, therefore, be explained as a weak localization effect, which should be characterized by a constant magnitude, independent of L_y.

B. Intrinsic domain wall magnetoconductance: sign reversal in coherent case

We define the intrinsic domain wall magnetoconductance as the difference between the conductance of a uniformly magnetized region ("uni") and that of a domain wall ("dw") of equal length with identical impurity configurations

$$\Delta g = g_{\mathrm{uni}} - g_{\mathrm{dw}}. \tag{28}$$

Assuming that we can contact the wall directly, the impurity average $\langle\Delta g\rangle$ could be associated with the change in the measured conductance when an external magnetic field along the z direction is applied in such a way as to destroy the domain wall and arrive at a magnetically homogeneous configuration. Although they are not of direct experimental relevance, we also define the differences in spin-dependent transmission, $\Delta T_\sigma = T^{(\mathrm{uni})}_\sigma - T^{(\mathrm{dw})}_\sigma$ in order to guide our physical discussion. With the above notations we obviously have $\Delta g = \Delta T_+ + \Delta T_-$.

In Fig. 5 we show the disorder-averaged $\langle\Delta g\rangle$ (thick lines, filled symbols) and $\langle\Delta T_\pm\rangle$ (thin lines, empty symbols) as a function of disorder, for spin-independent ($\rho=1$) and spin-dependent ($\rho=2$) disorder, in both coherent and incoherent cases.

In the spin-independent case [$\rho=1$, Fig. 5(a)], the main feature is a negative coherent magnetoconductance, which becomes positive and very small in the incoherent regime. For the spin-dependent case [$\rho=2$, Fig. 5(b)] the negative coherent magnetoconductance is obtained above a threshold disorder, and a positive $\langle\Delta g\rangle$ appears in the incoherent regime. Below we comment on the generality of these basic findings, their relationship with previously found effects, and their physical relevance.

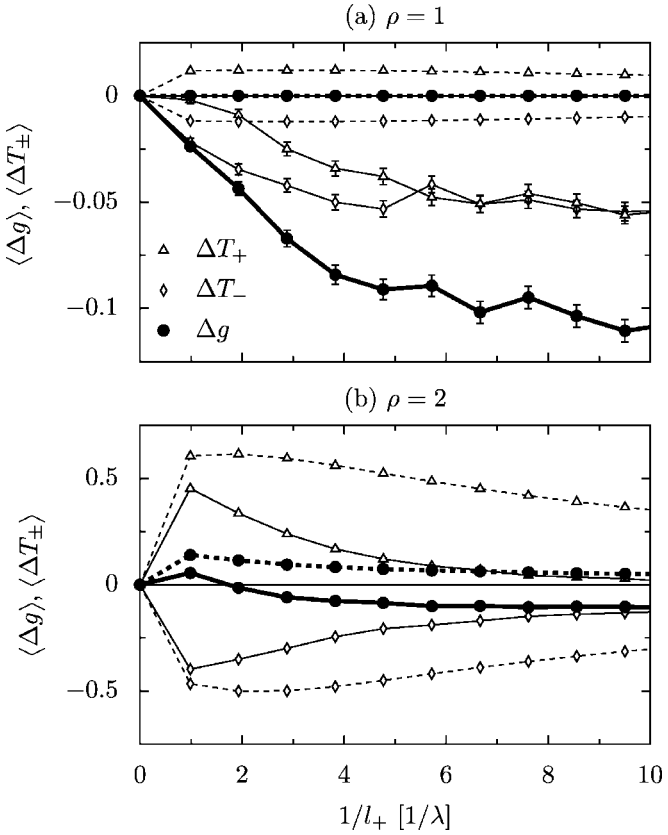

FIG. 5. Coherent (solid lines) and incoherent (dashed lines) domain wall magnetoconductance $\langle\Delta g\rangle$ (filled symbols) as a function of $1/l_+$ (in units of $1/\lambda$) for a domain wall with $p_{\mathrm{F}}=5$, in the case of (a) spin-independent disorder ($\rho=1$) and (b) spin-dependent disorder ($\rho=2$). The differences in spin-dependent transmission $\langle\Delta T_\pm\rangle$ are also shown (empty symbols). The system parameters are as for Fig. 4, with $N_{\mathrm{S}}=3000$ impurity configurations.

A negative coherent magnetoconductance was predicted by Tatara and Fukuyama[20,45] for the case of spin-independent disorder, and interpreted as a weak localization effect. Such an effect has, however, eluded experimental confirmation. The underlying reason for the putative reduction of weak localization in a domain wall is a suppression of backscattering processes which conserve spin. That is, $r_{\sigma n';\sigma n}$ is reduced due to the possibility of scattering into the opposite spin channel, $r_{-\sigma n';\sigma n}$. Since weak localization stems from an enhancement of the diagonal spin-conserving reflection amplitudes $r_{\sigma n;\sigma n}$ (coherent backscattering), it follows that the effect will be reduced in a domain wall as compared to a uniformly magnetized region.

Our numerical results suggest that a suppression of weak localization by the domain wall is indeed the dominant mechanism responsible for the coherent magnetoconductance in the regime of large disorder. First, the limiting value $\langle\Delta g_{\mathrm{co}}\rangle \simeq -0.1$, obtained in the diffusive regime, is of the order of the quasi-1D weak localization value of $-1/3$ for the uniform case.[27,40] Furthermore, this limiting value is approximately independent of system size (L_y and λ),[46] which is a general characteristic of coherence effects such as weak localization.

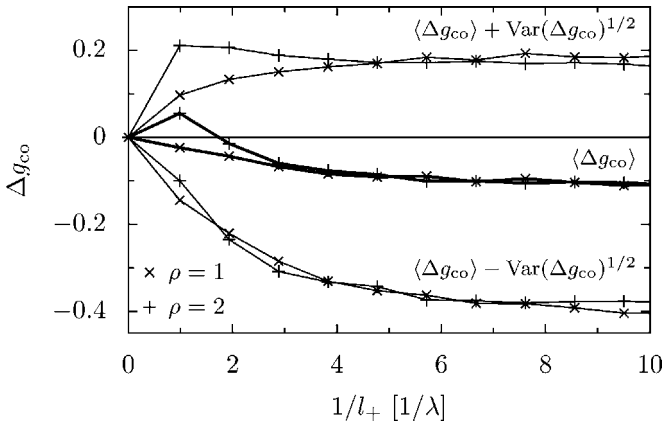

FIG. 6. Distribution of the coherent intrinsic magnetoconductance, Δg_{co}, for spin-independent ($\rho=1,\times$) and spin-dependent ($\rho=2,+$) disorder. The curves in the center show $\langle\Delta g_{co}\rangle$, while the upper and lower curves show $\langle\Delta g_{co}\rangle \pm \mathrm{Var}(\Delta g_{co})^{1/2}$, respectively. All parameters are as for Fig. 5.

From the point of view of physically measurable effects, it is important to note that the coherent magnetoconductance $\langle\Delta g_{co}\rangle$ is characterized by relatively large fluctuations. Indeed, in the diffusive regime Δg_{co} follows approximately a normal distribution with fluctuations characterized by $\sqrt{\mathrm{Var}(\Delta g_{co})}=(\langle\Delta g_{co}^2\rangle-\langle\Delta g_{co}\rangle^2)^{1/2}\simeq 0.3$, as illustrated in Fig. 6. For large disorder, the magnitude of these fluctuations is independent of system size (L_y) and up/down scattering ratio (ρ), and is related to the universal fluctuations of g_{dw} and g_{uni}. We discuss these aspects in more detail in the following section. We notice that $\sqrt{\mathrm{Var}(\Delta g_{co})}\simeq 3|\langle\Delta g_{co}\rangle|$ for large disorder. For an individual disorder configuration, there is thus a significant probability for Δg_{co} to be positive as well as negative. This could make it difficult for a negative $\langle\Delta g_{co}\rangle$ to be detected experimentally (even in the coherent regime) beyond statistical uncertainty.

Another significant factor concerning the coherent magnetoconductance is that in the case of spin-dependent disorder $\langle\Delta g_{co}\rangle$ is positive for small disorder. The value of $1/l_+$ at which it changes sign increases with the system width L_y. In our calculations, numerical constraints limit us to systems containing on the order of 10^2 channels. However, the nanowires of experiments such as Ref. 4 contain on the order of 10^4 channels. The region in which $\langle\Delta g_{co}\rangle$ is negative would then correspond to an unrealistically large disorder, particularly for the cobalt nanowires of Ref. 4, in which domain walls are relatively narrow ($\lambda\simeq 15$ nm). For materials with wider walls, such as nickel ($\lambda\simeq 100$ nm), the necessary density of impurity scatterers would be smaller, although it would be more difficult to have phase coherence across the greater length of the wall. Thus to access the regime of negative $\langle\Delta g_{co}\rangle$ experimentally it would be necessary to work with very small, highly disordered nanowires at low temperature.

In the incoherent regime, the magnetoconductance $\langle\Delta g_{inc}\rangle$ in the case of spin-independent disorder is positive but extremely small (approximately two orders of magnitude smaller than $|\langle\Delta T_{\pm,inc}\rangle|$). For spin-dependent disorder $\langle\Delta g_{inc}\rangle$ is much larger. Although not shown in Fig. 5, we note that the incoherent quantities scale linearly with increasing L_y, while for fixed $1/l_+$ they decrease with increasing λ (see Fig. 9).

The behavior of $\langle\Delta g_{inc}\rangle$ can be understood as a combination of spin-mistracking with spin-dependent scattering. As we saw in Sec. III A, successive scattering events in the domain wall enhance spin-mistracking. This means that the electron is sensitive not only to the impurity potential associated with its incoming spin, but also to the one with the opposite orientation. Since the scattering strengths are spin-dependent, this leads either to a reduction or enhancement of transmission compared to the uniform case, according to the spin direction: $\langle\Delta T_{+,inc}\rangle>0$ and $\langle\Delta T_{-,inc}\rangle<0$. For spin-independent disorder, these differences are small and almost equal in magnitude, so that $\langle\Delta g_{inc}\rangle$ is negligibly small. For spin-dependent disorder, however, we have $|\langle\Delta T_{+,inc}\rangle|>|\langle\Delta T_{-,inc}\rangle|$, which leads to a positive and much larger value of $\langle\Delta g_{inc}\rangle$. In this case there is thus a significant magnetoconductance arising from an enhancement of back-scattering due to the exposure of electrons in a superposition of spin states to spin-dependent scattering. This idea was used at a phenomenological level in Ref. 14, where transport through a diffusive domain wall in the almost adiabatic limit of small spin-mistracking was described by a reduced effective mean free path representing a weighted average between spin up and down mean free paths.

In the ballistic limit, $1/l_+\to 0$, there is no impurity scattering inside the wall. The backscattering is then entirely due to reflection from the wall interfaces, which is extremely weak. Both $\langle\Delta g_{co}\rangle$ and $\langle\Delta g_{inc}\rangle$ therefore become negligible in this limit.

In the diffusive regime ($\lambda/l_+\gg 1$), we believe that two primary mechanisms explain the different behavior of $\langle\Delta g_{co}\rangle$ and $\langle\Delta g_{inc}\rangle$. First, the limiting value of $\langle\Delta g_{co}\rangle$ for large disorder appears to be due to a reduction of weak localization by the domain wall, which does not apply in the incoherent case. Second, as we discussed in Sec. III A, the spin-mistracking transmission and reflection, $\langle T^{(dw)}_{-\sigma\sigma,co}\rangle$ and $\langle R^{(dw)}_{-\sigma\sigma,co}\rangle$, are reduced in the coherent regime with respect to the incoherent one. We propose that this leads to a suppression of the enhanced backscattering in the domain wall which is dominant in the incoherent case. For large disorder, the positive magnetoconductance present in the incoherent case is then canceled out in the coherent case, leaving only the negative component from the weak localization reduction.

As stated in the presentation of our physical model (Sec. II), reducing the transverse cross section of the wire from two to one dimensions is not expected to change the physics of the problem. This is true as long as we are in a quasi-1D geometry where the length of the disordered system is much larger than its transverse dimensions. In this situation only the lowest transverse diffusion modes are relevant[40] and the universal quasi-1D value of $-1/3$ is obtained for the weak localization correction in the absence of a domain wall.

C. Reduction of universal conductance fluctuations for coherent domain wall

An important feature of quantum transport through diffusive coherent systems is that the conductance fluctuations, $(\delta g^2)^{1/2}=\mathrm{Var}(g)^{1/2}$, are *universal*, with a magnitude of order e^2/h independent of the system size or mean free path.[47] For a spinless quasi-1D disordered system, the conductance fluctuations have the value $\sqrt{2/15}$ in units of e^2/h. In our model this applies to each spin subband in the uniformly magnetized case, so that

$$(\delta[T_{\pm}^{(\mathrm{uni})}]^2)^{1/2}=\sqrt{2/15}. \tag{29}$$

For a nonmagnetic system ("nm"), there is no spin-splitting of the s band (which would correspond to $\Delta=0$ in our model) and the transport of up and down electrons is identical. In that case we have $T_{+}^{(\mathrm{nm})}=T_{-}^{(\mathrm{nm})}$ and hence $(\delta[T_{+}^{(\mathrm{nm})}+T_{-}^{(\mathrm{nm})}]^2)^{1/2}=2(\delta[T_{+}^{(\mathrm{nm})}]^2)^{1/2}$. The conductance fluctuations are then

$$(\delta g_{\mathrm{nm}}^2)^{1/2}=2(\delta[T_{+}^{(\mathrm{nm})}]^2)^{1/2}=\sqrt{8/15}. \tag{30}$$

In a ferromagnetic system ($\Delta\neq 0$), on the other hand, the spin dependence of the wave vectors $k_{\sigma n}$ suppresses the correlation between $T_{+}^{(\mathrm{uni})}$ and $T_{-}^{(\mathrm{uni})}$. In this case we have $(\delta[T_{+}^{(\mathrm{uni})}+T_{-}^{(\mathrm{uni})}]^2)^{1/2}=(2\delta[T_{+}^{(\mathrm{uni})}]^2)^{1/2}$, so the conductance fluctuations are reduced as compared to those of a nonmagnetic system:

$$(\delta g_{\mathrm{uni}}^2)^{1/2}=(2\delta[T_{+}^{(\mathrm{uni})}]^2)^{1/2}=\sqrt{4/15}. \tag{31}$$

This reduction due to the nondegeneracy of spin states is directly analogous to the experimentally observed reduction of conductance fluctuations due to Zeeman splitting in an applied magnetic field.[27]

In Fig. 7(a) we show the conductance fluctuations obtained from our model in the uniform case, $(\delta g_{\mathrm{uni}}^2)^{1/2}$ and $(\delta[T_{\pm}^{(\mathrm{uni})}]^2)^{1/2}$, as a function of $1/l_{+}$. They are in excellent agreement with the theoretical values from Eqs. (29) and (31) for $\lambda/l_{+}\gtrsim 2$.

Figure 7(a) also shows the conductance fluctuations for a domain wall region, $(\delta g_{\mathrm{dw}}^2)^{1/2}$, together with $(\delta[T_{\pm}^{(\mathrm{dw})}]^2)^{1/2}$. We see that the conductance fluctuations in a disordered domain wall are reduced with respect to those of a uniformly magnetized region. Moreover, the conductance fluctuations are no longer universal since a slow decrease is observed as a function of $1/l_{+}$ in the diffusive regime.

This result can be understood as arising from statistical decorrelation between the components of $T_{\sigma}^{(\mathrm{dw})}$. For the domain wall coefficients $T_{\sigma'\sigma}^{(\mathrm{dw})}$ we do not have a way of estimating the fluctuations analogous to Eq. (29). However, we can make the hypothesis that the relative fluctuations for each component are the same as in the uniform case:

$$\frac{(\delta[T_{\sigma'\sigma}^{(\mathrm{dw})}]^2)^{1/2}}{\langle T_{\sigma'\sigma}^{(\mathrm{dw})}\rangle}\simeq\frac{(\delta[T_{\sigma}^{(\mathrm{uni})}]^2)^{1/2}}{\langle T_{\sigma}^{(\mathrm{uni})}\rangle}. \tag{32}$$

Furthermore, we can expect that $T_{\sigma\sigma}^{(\mathrm{dw})}$ and $T_{-\sigma\sigma}^{(\mathrm{dw})}$ will be uncorrelated in the diffusive regime, so that

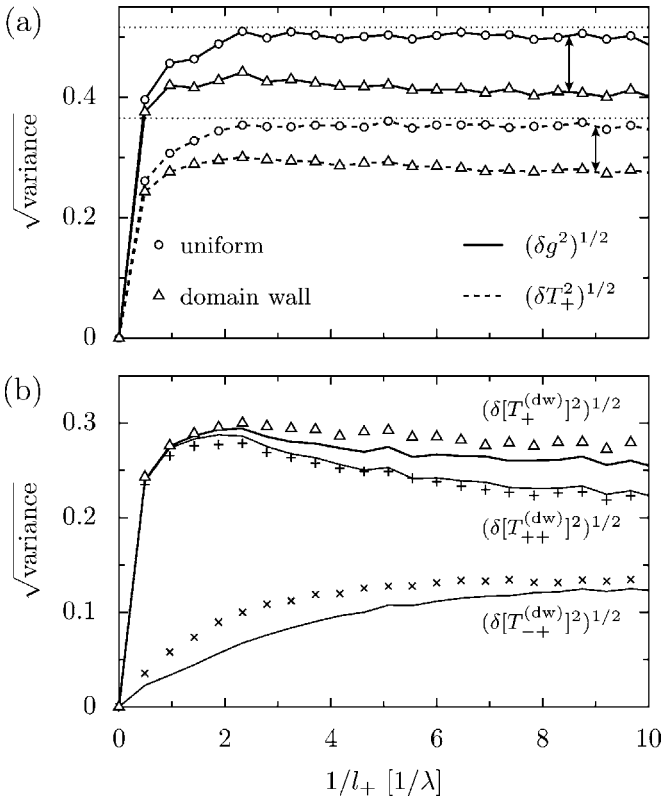

FIG. 7. (a) Fluctuations of conductance, $(\delta g^2)^{1/2}$ (solid lines), and spin-dependent transmission, $(\delta T_{+}^2)^{1/2}$ (dashed lines), for a uniformly magnetized region (○) and domain wall (△), in the case of spin-independent disorder ($\rho=1$). The fluctuations of spin-down transmission $(\delta T_{-}^2)^{1/2}$ are not shown, but agree with $(\delta T_{+}^2)^{1/2}$ to within the statistical error of the calculation. The dotted horizontal lines indicate the theoretical values in the uniform case, $(\delta g_{\mathrm{uni}}^2)^{1/2}=\sqrt{4/15}$ and $(\delta[T_{\pm}^{(\mathrm{uni})}]^2)^{1/2}=\sqrt{2/15}$, which are in good agreement with our numerical results for $\lambda/l_{+}\gtrsim 2$. (b) Fluctuations of the spin-dependent domain wall transmission coefficients: $(\delta[T_{+}^{(\mathrm{dw})}]^2)^{1/2}$ (△), $(\delta[T_{++}^{(\mathrm{dw})}]^2)^{1/2}$ (+), and $(\delta[T_{-+}^{(\mathrm{dw})}]^2)^{1/2}$ (×). The corresponding estimated values, based on the approximation in Eqs. (32)–(34), are also shown (solid lines). System parameters are $p_{\mathrm{F}}=5$ and $L_y=10$ nm, with 3000 impurity configurations.

$$(\delta[T_{\sigma}^{(\mathrm{dw})}]^2)^{1/2}\simeq(\delta[T_{\sigma\sigma}^{(\mathrm{dw})}]^2+\delta[T_{-\sigma\sigma}^{(\mathrm{dw})}]^2)^{1/2}. \tag{33}$$

Using the fact that $\langle T_{\sigma}^{(\mathrm{dw})}\rangle=\langle T_{\sigma\sigma}^{(\mathrm{dw})}\rangle+\langle T_{-\sigma\sigma}^{(\mathrm{dw})}\rangle$, Eqs. (32) and (33) then give

$$(\delta[T_{\sigma}^{(\mathrm{dw})}]^2)^{1/2}\simeq\frac{\langle T_{\sigma}^{(\mathrm{dw})}\rangle}{\langle T_{\sigma}^{(\mathrm{uni})}\rangle}\left(1-\frac{2\langle T_{\sigma\sigma}^{(\mathrm{dw})}\rangle\langle T_{-\sigma\sigma}^{(\mathrm{dw})}\rangle}{\langle T_{\sigma}^{(\mathrm{dw})}\rangle^2}\right)^{1/2}(\delta[T_{\sigma}^{(\mathrm{uni})}]^2)^{1/2}. \tag{34}$$

The first factor on the right-hand side (rhs) is approximately unity since $\langle T_{\sigma}^{(\mathrm{dw})}\rangle\simeq\langle T_{\sigma}^{(\mathrm{uni})}\rangle$. We thus see that $(\delta[T_{\sigma}^{(\mathrm{dw})}]^2)^{1/2}$ is reduced with respect to $(\delta[T_{\sigma}^{(\mathrm{uni})}]^2)^{1/2}$ by the second term on the rhs of Eq. (34). This reduction factor is most important when the two transmission coefficients $\langle T_{\sigma\sigma}^{(\mathrm{dw})}\rangle$ and $\langle T_{-\sigma\sigma}^{(\mathrm{dw})}\rangle$ are of the same order, which is the situation approached with increasing disorder.

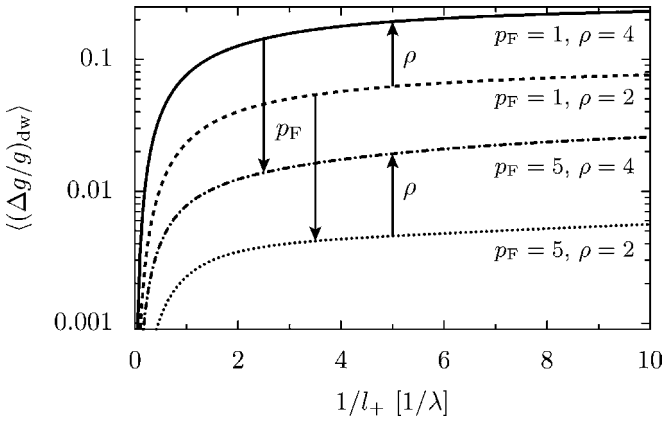

FIG. 8. Intrinsic relative domain wall magnetoconductance, $\langle(\Delta g/g)_{\rm dw}\rangle$, as a function of disorder strength, $1/l_+$ (in units of $1/\lambda$), in the incoherent case. The different curves illustrate the dependence on wall width ($p_{\rm F}=1,5$) and spin dependence of scattering ($\rho=2,4$). The arrows indicate the evolution of the curves upon increasing these parameters. Other system parameters are as for Fig. 4.

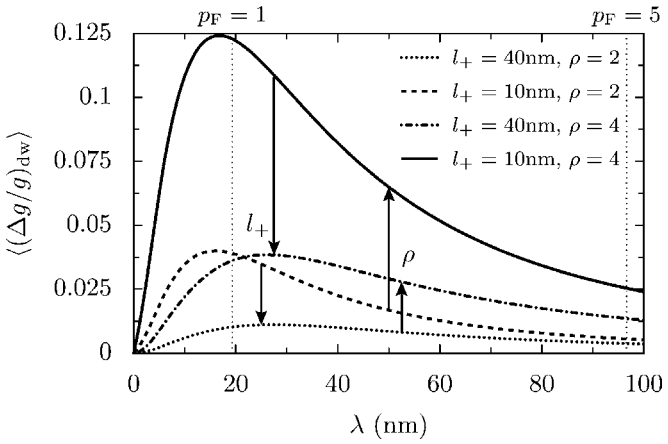

FIG. 9. Intrinsic relative domain wall magnetoconductance, $\langle(\Delta g/g)_{\rm dw}\rangle$, as a function of wall width, λ, in the incoherent case. Several values of mean free path ($l_+=10$ and 40 nm) and spin dependence of scattering ($\rho=2,4$) are shown. The arrows show the direction in which the curves evolve upon increasing these parameters. The two values of wall width corresponding to Fig. 8 ($p_{\rm F}=1,5$) are indicated by dotted vertical lines. Other system parameters are as for Fig. 4.

In Fig. 7(b) we compare the actual fluctuations $(\delta[T_\sigma^{(\rm dw)}]^2)^{1/2}$ and $(\delta[T_{\sigma'\sigma}^{(\rm dw)}]^2)^{1/2}$ with the corresponding predictions of Eq. (34). The two agree reasonably well and, significantly, the approximate values reproduce the decreasing behavior of $(\delta[T_\sigma^{(\rm dw)}]^2)^{1/2}$ for $1/l_+$ large. The simple hypotheses contained in Eqs. (32) and (33) thus explain qualitatively the two essential features of $(\delta[T_\sigma^{(\rm dw)}]^2)^{1/2}$, which are an overall reduction with respect to $(\delta[T_\sigma^{(\rm uni)}]^2)^{1/2}$ and a loss of universality represented by a slow decrease with increasing disorder.

D. Nonmonotonic λ-dependence of incoherent relative magnetoconductance

We now consider the relative intrinsic domain wall magnetoconductance, defined as

$$(\Delta g/g)_{\rm dw} = \frac{g_{\rm uni} - g_{\rm dw}}{g_{\rm uni}}. \tag{35}$$

For disordered systems this is a more useful quantity than the magnetoconductance Δg discussed in Sec. III B, as it measures the *relative* importance of the magnetoconductance effect inside the wall. In this section we consider only the incoherent regime; for this case, $(\Delta g/g)_{\rm dw}$ is independent of L_y since $\langle\Delta g_{\rm inc}\rangle$ scales linearly with transverse system size.

In Fig. 8 we plot $\langle(\Delta g/g)_{\rm dw}\rangle$ as a function of $1/l_+$ (in units of $1/\lambda$). Various domain wall widths ($p_{\rm F}=1,5$) and up/down scattering ratios ($\rho=2,4$) are shown. We see that $\langle(\Delta g/g)_{\rm dw}\rangle$ *is a monotonically increasing function of disorder*. This shows that the decreasing behavior of $\langle\Delta g_{\rm inc}\rangle$ for large disorder is due simply to the overall decrease in conductance with disorder. The monotonicity of $\langle(\Delta g/g)_{\rm dw}\rangle$ occurs because the amount of spin-mistracking, and hence also the enhancement of backscattering, is proportional to the amount of impurity scattering, as discussed in Sec. III B. It can also be seen from Fig. 8 that $\langle(\Delta g/g)_{\rm dw}\rangle$ increases with ρ and decreases with $p_{\rm F}$, which is consistent with the explanation of the intrinsic magnetoconductance given in Sec. III B.

We note that the models of Refs. 14 and 18 assume diffusive transport, so that the results obtained therein correspond to the regime of large $1/l_+$ in Fig. 8. The magnetoconductance predicted in these works depends on the up/down scattering ratio ρ, but is independent of l_+ (provided it satisfies $l_+ \ll \lambda$). This is consistent with the leveling off of the curves in Fig. 8 with increasing $1/l_+$, and suggests that $\langle(\Delta g/g)_{\rm dw}\rangle$ approaches a finite limit for large disorder.

Figure 9 shows $\langle(\Delta g/g)_{\rm dw}\rangle$ as a function of wall width λ, for $\rho=2$ and 4 and $l_+=10$ and 40 nm. For large λ, we find a $1/\lambda$ dependence in agreement with Refs. 14 and 18. This can be understood because with increasing wall width the amount of spin-mistracking is reduced. In the limit $\lambda \to 0$, on the other hand, the domain wall becomes an abrupt interface with no impurities and $\langle(\Delta g/g)_{\rm dw}\rangle$ becomes negligible. As discussed in Sec. II B 1, the channel blocking mechanism[10,15] which typically yields $\Delta g/g \sim \Delta/E_{\rm F}$ is not relevant in our case since we have chosen $N_+=N_-$. In between the two extreme cases, *there must be a maximum value of* $\langle(\Delta g/g)_{\rm dw}\rangle$ *at a finite value of* λ. This value represents an optimum intermediate situation: a wall which is wide enough to contain an appreciable amount of impurity scattering, but narrow enough to cause significant spin-mistracking. From Fig. 9 it can be inferred that this value of λ decreases with increasing disorder (i.e., decreasing l_σ). On the other hand, the different values of ρ affect the overall magnitude of $\langle(\Delta g/g)_{\rm dw}\rangle$, but do not significantly change the position of its maximum value.

IV. DOMAIN WALL IN A NANOWIRE: EFFECT OF SCATTERING IN THE LEADS

To understand the effect of a domain wall on electron transport in a nanowire, it is necessary to consider not only

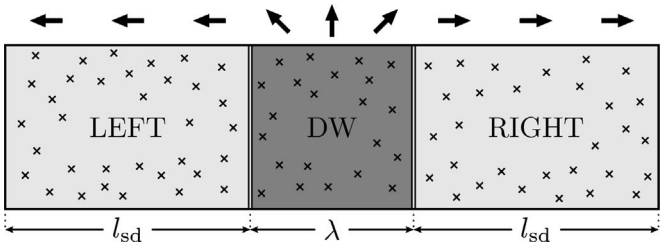

FIG. 10. Diagram illustrating the physical region considered in Sec. IV. On either side of the domain wall are uniformly magnetized regions of length l_{sd} representing the distance over which electrons propagate before spin relaxation.

the *intrinsic* effects described in the previous section, but also *extrinsic* effects arising from scattering in the regions adjacent to the wall. In a previous work[16] we analyzed such effects in the special case of a ballistic domain wall, using a circuit model which incorporates spin-dependent scattering in the regions on either side of the wall using a generalization of the two-resistor model of GMR.[17] The essence of this model is to treat transport of electrons with different spins in the adjacent regions as independent over a distance equal to the spin-diffusion length, l_{sd}. This is the length scale over which the distribution between the two spin subbands is equilibriated through spin-flip scattering processes. In Ref. 16, transport in the adjacent regions was treated using classical spin-dependent resistors. Such an approach is valid under the assumption that the phase coherence length, L_ϕ, satisfies $\lambda \lesssim L_\phi \ll l_{sd}$.

In this section we follow a similar method to incorporate extrinsic scattering (outside the domain wall region) into our model. However, in place of classical spin-dependent resistors, we treat the impurity scattering in the regions adjacent to the domain wall using the same delta function scatterer model as inside the domain wall. The resulting model system is illustrated in Fig. 10. This approach differs with respect to Ref. 16 in that the adjacent regions are combined with the domain wall using the scattering matrix combination formula [Eqs. (9)], rather than combining spin-dependent conductances using Kirchhoff's rules. We are interested in the limit $l_\pm \ll l_{sd}$, for which the difference between these two approaches is not significant. This corresponds to the realistic situation since only a small part of the processes leading to momentum relaxation involve a spin-flip. However, the present approach has the advantage that it remains valid in principle for any value of $l_\pm / l_{sd}$. In addition, phase coherence lengths $L_\phi > \lambda$ can be considered within this approach (although we do not do so in this paper).

As in Sec. III, we consider conductance through the domain wall in both coherent and incoherent cases. In the coherent case we introduce a finite $L_\phi = \lambda$. The system is thus partitioned into phase-coherent segments of length L_ϕ which are combined incoherently. For the incoherent case, our approach assumes a vanishing phase coherence length, so no partitioning is necessary.

The physical system in Fig. 10 has total length $L_{wire} = 2l_{sd} + \lambda$. We will refer to this system as "the wire" since, by assumption, the transport outside this region is in equilibrium between the two spin channels and therefore does not contribute to magnetoconductance effects. Our main interest will be the relative magnetoconductance for the wire, $(\Delta g/g)_{wire}$, which is defined analogously to Eq. (35) by changing the intrinsic domain wall conductances to combined wire conductances.

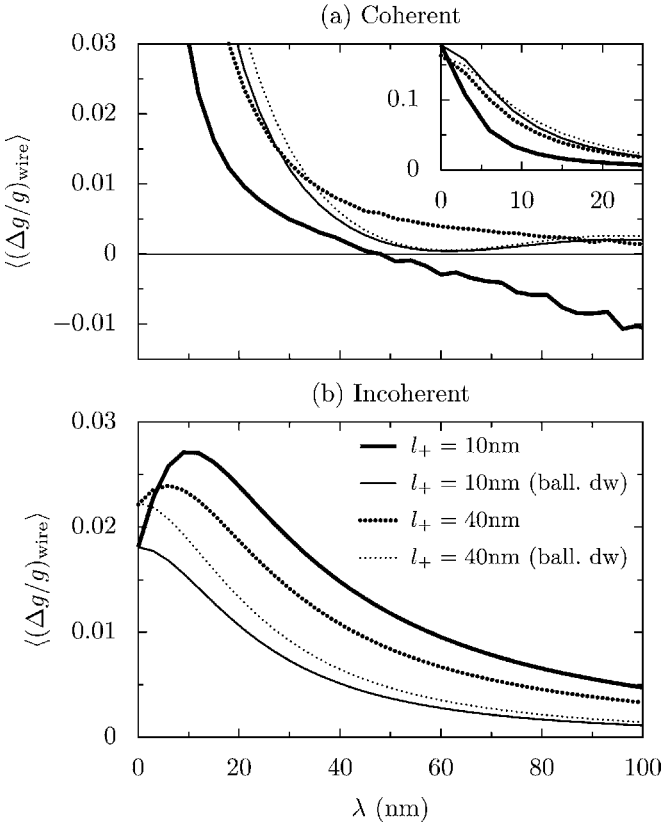

FIG. 11. Magnetoconductance of a domain wall in a nanowire, $\langle(\Delta g/g)_{wire}\rangle$, as a function of wall width λ for (a) coherent and (b) incoherent transport through the domain wall region. Two values of mean free path are shown, $l_+ = 10$ and 40 nm (thick lines). The magnetoconductance of an equivalent disordered wire with a ballistic domain wall (i.e., no impurities inside the wall) is also shown (thin lines). The inset in the upper figure shows the coherent $\langle(\Delta g/g)_{wire}\rangle$ in the small λ region. Other parameter values are $L_y = 5$ nm, $\rho = 2$, and $l_{sd} = 4l_+$, with $N_S = 3000$ impurity configurations.

A. Domain wall magnetoconductance in a wire: Effect of disorder inside domain wall

In Fig. 11 (thick lines) we show $\langle(\Delta g/g)_{wire}\rangle$ as a function of domain wall width λ for both coherent and incoherent cases. To illustrate the dependence on disorder, two values of mean free path are shown ($l_+ = 10$ and 40 nm). In all cases we fix $\rho = 2$ and $l_{sd} = 4l_+$. Results for other values of these parameters are qualitatively unchanged. A special case is the limit $\rho \to 1$: here the scattering is independent of spin and hence, as for the intrinsic case of Sec. III, the magnetoconductance effect becomes very small. For comparison with our previous work,[16] in which the domain wall was treated as ballistic, Fig. 11 also shows the magnetoconductance for the equiva-

lent wire with no scatterers inside the domain wall (thin lines).

In the narrow wall limit, $\lambda \to 0$, the coherent regime is the physically relevant one. Figure 11(a) shows that the coherent $\langle(\Delta g/g)_{\text{wire}}\rangle$ (solid lines) *tends to a maximum value as* $\lambda \to 0$. This is in contrast to the behavior of the intrinsic magnetoconductance $\langle \Delta g \rangle$ studied in the previous section, which (for both coherent and incoherent cases) goes to zero in this limit. From our previous work,[16] this result is expected since at $\lambda = 0$ the wall corresponds to a GMR interface,[17] for which there is complete mistracking of spin. It is interesting to note, however, that for small but nonzero λ, $\langle(\Delta g/g)_{\text{wire}}\rangle$ is reduced for a coherent wall with disorder [Fig. 11(a), thick lines] compared to a ballistic wall (Fig. 11, thin lines). Therefore, when scattering in the surrounding regions is taken into account, the presence of disorder inside the wall reduces the magnetoconductance effect of narrow domain walls.

In the incoherent regime, the magnetoconductance is significantly reduced with respect to the coherent regime in the limit $\lambda \to 0$. Furthermore, it is a nonmonotonic function of disorder in this limit, having a maximum value at a wall width $\lambda > 0$. In fact, this behavior is an artifact arising from the lack of complete mistracking when $\lambda \to 0$ for transmission through an incoherent wall, which we discussed in Sec. II B 1. As we mentioned above, in this limit the coherent regime describes the physical situation, so these effects are not physically relevant.

In the wide wall limit $\lambda \to \infty$, the behavior of $\langle(\Delta g/g)_{\text{wire}}\rangle$ is qualitatively similar to that of $\langle(\Delta g/g)_{\text{dw}}\rangle$ of Sec. III. The coherent magnetoconductance is significantly reduced with respect to the incoherent one and becomes negative for large λ [in Fig. 11(a) this is most evident for $l_+ = 10$ nm]. These effects are due to the intrinsic properties of coherent transport through a disordered domain wall which we discussed in Sec. III B.

For large λ the incoherent regime is the physically relevant one. In this case the magnetoconductance decreases as $1/\lambda^2$, which is the same parametric behavior as the intrinsic case (Sec. III D). However, we will see in the next section that this effect is larger in magnitude for $\langle(\Delta g/g)_{\text{wire}}\rangle$. In this case, comparison between the incoherent disordered wall [Fig. 11(b), thick lines] with an incoherent ballistic wall [Fig. 11(b), thin lines] shows that the presence of disorder inside the wall enhances the magnetoconductance effect in wide domain walls. This enhancement has two causes. First, for a disordered wall there is an intrinsic contribution due to scattering from impurities inside the wall, which is absent in the case of a ballistic wall. Second, the disordered wall gives rise to an enhanced spin-mistracking (Sec. III A), which leads to an increase in the GMR scattering in the surrounding regions.

To our knowledge no experimental data exists comparing the conductance through domain walls in wires with different amounts of disorder; the findings of this section suggest that such a difference may be observable.

B. Enhancement of domain wall magnetoconductance from extrinsic scattering

The total magnetoconductance of a wire containing a domain wall, $(\Delta g/g)_{\text{wire}}$, arises from scattering effects which may be classified as either *intrinsic* or *extrinsic*. Intrinsic effects are those due to scattering occurring within the region of the domain wall itself, and are characterized by the intrinsic magnetoconductance $(\Delta g/g)_{\text{dw}}$ studied in Sec. III D. Extrinsic effects, on the other hand, occur in the regions adjacent to the domain wall, and arise from a GMR-like enhancement of backscattering due to the spin-mistracking of electrons scattered by the wall.

We now determine the relative importance of intrinsic and extrinsic effects in the magnetoconductance of a domain wall in a nanowire. In order to do this, we compare $(\Delta g/g)_{\text{wire}}$, which contains both intrinsic and extrinsic effects, with $(\Delta g/g)_{\text{dw}}$, which contains only intrinsic ones.

In the narrow wall limit, $\lambda \to 0$, the amount of impurity scattering inside the wall goes to zero, and hence $\langle(\Delta g/g)_{\text{dw}}\rangle$ becomes negligible. On the other hand, Fig. 11 shows that, in the physically relevant case of coherent walls, $\langle(\Delta g/g)_{\text{wire}}\rangle$ achieves its maximum value in this limit. It is therefore clear that for narrow walls, extrinsic scattering effects are the dominant mechanism underlying the domain wall magnetoconductance.

For general λ, however, the situation is more complicated. We saw in Sec. III D that $\langle(\Delta g/g)_{\text{dw}}\rangle$ is significant for disordered walls. At the same time, the scattering from impurities inside the wall enhances the spin-mistracking of transmitted and reflected electrons (Sec. III A), which will lead to extrinsic scattering. We therefore expect that both intrinsic and intrinsic effects will be significant in general. To determine the relative magnitude of the two, it is necessary to compare $\langle(\Delta g/g)_{\text{wire}}\rangle$ and $\langle(\Delta g/g)_{\text{dw}}\rangle$ quantitatively.

For this comparison we need to "renormalize" $(\Delta g/g)_{\text{dw}}$ to describe the same total system size as the wire, i.e., $L_{\text{wire}} = 2l_{\text{sd}} + \lambda$. To do this, we calculate separately the *total* conductances (summed over all spin and transverse channels) for each of the three regions of the wire: the domain wall (g_{dw}), and the two surrounding regions (g_{left} and g_{right}). Taking the incoherent combination of the three regions[35] we then obtain a total conductance g_{int} over the length of the wire:

$$\frac{1 - g_{\text{int}}}{g_{\text{int}}} = \frac{1 - g_{\text{left}}}{g_{\text{left}}} + \frac{1 - g_{\text{dw}}}{g_{\text{dw}}} + \frac{1 - g_{\text{right}}}{g_{\text{right}}}. \tag{36}$$

Combining conductances in this way is equivalent to making the assumption that the two spin channels are equilibriated at the wall boundaries rather than at a distance l_{sd} from the wall.

By comparing g_{int} with the conductance of a uniform region of length $2l_{\text{sd}} + \lambda$, we calculate an "intrinsic" magnetoconductance $(\Delta g/g)_{\text{int}}$. This quantity represents the desired renormalization of $(\Delta g/g)_{\text{dw}}$ to the length L_{wire}. We note that for $l_+ \ll \lambda$ this can be calculated approximately as

$$(\Delta g/g)_{\text{int}} = \frac{\lambda}{2l_{\text{sd}} + \lambda}(\Delta g/g)_{\text{dw}}. \tag{37}$$

In Fig. 12 we show the ratio of $\langle(\Delta g/g)_{\text{wire}}\rangle$ and $\langle(\Delta g/g)_{\text{int}}\rangle$ as a function of λ for several values of ρ and l_{sd}, in the incoherent case. We see that the ratio is largest in the

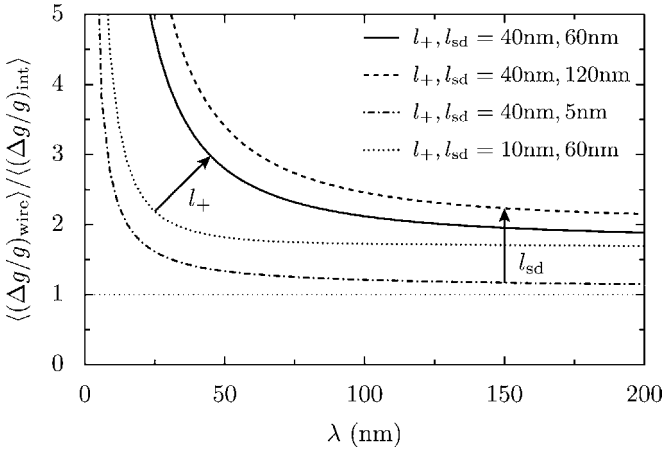

FIG. 12. Ratio of incoherent wire and intrinsic domain wall magnetoconductance $\langle(\Delta g/g)_{wire}\rangle/\langle(\Delta g/g)_{int}\rangle$ as a function of λ, for illustrative values of l_+ and l_{sd}. The system parameters are $\rho=2$ and $L_y=10$ nm.

limit of small λ. As we mentioned previously, this is because $\langle(\Delta g/g)_{dw}\rangle$ becomes negligible in the limit $\lambda\to 0$ while $\langle(\Delta g/g)_{wire}\rangle$ becomes large. We note that the ratios shown in Fig. 12 apply to the incoherent regime. As we saw in Fig. 11, $\langle(\Delta g/g)_{wire}\rangle$ is much larger near $\lambda\to 0$ for the coherent case than for the incoherent one. Therefore in the coherent case the corresponding enhancement of $\langle(\Delta g/g)_{wire}\rangle$ with respect to $\langle(\Delta g/g)_{int}\rangle$ will also be larger.

For large λ, Fig. 12 shows the less obvious result that $\langle(\Delta g/g)_{wire}\rangle$ is substantially larger than $\langle(\Delta g/g)_{int}\rangle$ even in the case of wide walls ($\lambda\simeq 200$ nm). The ratio depends on the parameter values, and for those of Fig. 12 it is between ~ 1.2 (unrealistically small l_{sd}, shown for comparison) and ~ 2.2 (large l_{sd}) at $\lambda=200$ nm. We thus see that extrinsic spin-dependent scattering effects are quantitatively important for domain wall magnetoconductance, even for wide walls. This is an important point, since the most widely accepted existing models[14,18,20] consider conductance only through the region of the wall, and hence ignore extrinsic effects.

V. CONCLUSION

In this work we have studied spin-dependent electron transport through domain walls in disordered ferromagnetic nanowires. Using a numerical scattering matrix formalism, we considered a large range of impurity concentrations, corresponding to transport regimes from ballistic through to diffusive. In addition, our approach allowed us to consider spin-dependent impurity scattering, and to distinguish between the fully coherent and fully incoherent transport regimes.

The contribution of a domain wall to the resistance of a wire is due to two main mechanisms. The first one is the reflection of electrons from the domain wall itself and impurities within the domain wall region. The second is related to the spin-dependent resistivity of the wire regions surrounding the domain wall. We therefore considered first the spin-dependent "intrinsic" transport coefficients of the disordered domain wall region itself, and then showed in the last section what can be expected for the resistance of the whole wire, which is the experimentally measurable quantity.

The intrinsic effects stem from the presence of impurities inside a domain wall, which causes electrons to be scattered both with and without spin reversal. This leads to an enhancement of backscattering caused by exposure of electrons in a superposition of spin states to spin-dependent scattering. In the incoherent regime this gives rise to a reduction of the intrinsic domain wall conductance. The maximum reduction occurs at a disorder-dependent value of the domain wall length.

In the phase-coherent regime, the relative amount of reflection with spin reversal is reduced with respect to the incoherent regime. For large disorder, this acts to suppress the backscattering enhancement observed in the incoherent case. Indeed, the overall effect in this regime is an enhancement of *transmission* through the domain wall. This can be understood as arising from a suppression of weak localization by the domain wall, which is consistent with the findings of Ref. 20. However, there are several reasons why such a behavior would be difficult to observe experimentally. In particular, the fluctuations of the magnetoconductance are large relative to its average value, which means that both positive and negative values may be observed for individual samples. Nevertheless, our analysis suggests that a negative magnetoconductance effect may be observable experimentally, provided that one works with highly disordered systems at low temperatures. If, while staying below the phase coherence length, the wall width exceeds a critical length that decreases with disorder, a negative magnetoresistance should appear. In principle, this effect may therefore be observable in a variety of materials.

The mesoscopic character of the transport in the coherent regime is underlined by a study of the conductance fluctuations. For a domain wall it is found that these are reduced with respect to the uniformly magnetized case, as a result of decorrelation between the components of a given incoming spin state which are transmitted with and without reversal of spin. Furthermore, the sample-dependent fluctuations of the domain wall contribution to the resistance can be significantly larger than its average value in the diffusive limit. This should be kept in mind when experiments on individual samples approach the coherent regime.

To address the experimentally measurable conductance of a disordered nanowire containing a domain wall, we included in our treatment uniformly magnetized regions of length l_{sd} (the spin diffusion length) on either side of the domain wall. Since the phase coherence length does not exceed l_{sd}, the rest of the wire is taken into account as a classical resistance in series that does not contribute to the magnetoconductance.

The spin-dependent scattering in the regions adjacent to the wall results in an enhancement of the resistance. This arises from processes in which the spin of the electrons does not follow the domain wall magnetization while they propagate through the wall. The spin-dependent scattering in the surrounding regions contributes an "extrinsic" domain wall resistance effect which is similar in nature to giant magnetoresistance. This mechanism is distinct from the intrinsic effect occurring inside the wall.

As compared to the intrinsic domain wall resistance alone, the total resistance due to a domain wall in a nanowire is significantly enhanced by the extrinsic scattering. The enhancement is most dramatic for narrow walls, where the intrinsic resistance becomes negligible. However, it remains important (a factor of 2 for typical parameters) even for wide walls.

In our previous study based on ballistic domain walls in a circuit model[16] we found results in order-of-magnitude agreement with a recent experiment.[4] The relevant regime for this experiment is intermediate between the coherent and incoherent regimes, and corresponds to domain walls far from the adiabatic limit of zero spin-mistracking. In the present work, we have found that the presence of disorder inside the wall in this regime leads to a quantitative reduction of the magnetoconductance effect as compared to the ballistic wall used in Ref. 16, but is still within an order of magnitude of the experiment. This is acceptable given the uncertainties over various physical parameters relevant for the experiment (such as the precise value of the elastic mean free path). On the other hand, in the case of wide walls in the incoherent transport regime, we have found that disorder enhances the magnetoconductance effect. This regime is relevant for experiments in materials such as nickel and iron. Our model should also be applicable to the understanding of recent measurements of domain wall resistance in ferromagnetic semiconductors.[50]

In both narrow and wide wall regimes, our results show that disorder inside and outside a domain wall leads to important effects in the magnetoconductance. Since disorder is unavoidable in mesoscopic wires, our conclusions should be testable experimentally.

ACKNOWLEDGMENTS

P.E.F. is grateful for the support of an Australian Postgraduate Award and a Jean Rogerson Fellowship from the University of Western Australia and for support from the Université Louis Pasteur in Strasbourg. This work was also supported through the Australian Research Council Linkages and Discovery Programmes and by the European Union through the RTN programme. R.A.J. and D.W. acknowledge the hospitality of the Physics Department of the University of Western Australia, where part of this work was done with financial support from the ARC (R.A.J.) and the DREI of the CNRS (D.W.).

APPENDIX A: SCATTERING MATRIX OF DOMAIN WALL INTERFACES

In this appendix we present formulas for the calculation of the scattering matrices of the domain wall interfaces $\tilde{s}^{(\mathrm{L,R})}$. These are obtained by forming scattering state solutions from the basis states of Eqs. (5) and (17) for each side of the interface and matching the functions and their derivatives at $z=0$ (left interface) or $z=\lambda$ (right interface). For the domain wall interfaces the matrix elements corresponding to scattering between different transverse modes, $n' \neq n$, are zero since the domain wall profile depends only on the longitudinal coordinate. The amplitudes $\tilde{r}^{(\mathrm{L,R})}_{\pm\sigma n;\sigma n}$, $\tilde{t}^{(\mathrm{L,R})}_{\pm\sigma n;\sigma n}$ and $\tilde{r}'^{(\mathrm{L,R})}_{\pm\sigma n;\sigma n}$, $\tilde{t}'^{(\mathrm{L,R})}_{\pm\sigma n;\sigma n}$ satisfy 4×4 sets of equations. The equations for $\tilde{r}^{(\mathrm{L})}_{\sigma' n;\sigma n}$ and $\tilde{t}^{(\mathrm{L})}_{\sigma' n;\sigma n}$ read (for clarity we omit the n and L labels)

$$1+\tilde{r}_{\sigma\sigma}=\sqrt{\frac{v_\sigma}{\tilde{v}_\sigma}}\tilde{t}_{\sigma\sigma}+iA_{-\sigma}\sqrt{\frac{v_\sigma}{\tilde{v}_{-\sigma}}}\tilde{t}_{-\sigma\sigma}, \tag{A1a}$$

$$\sqrt{\frac{v_\sigma}{v_{-\sigma}}}\tilde{r}_{-\sigma\sigma}=iA_\sigma\sqrt{\frac{v_\sigma}{\tilde{v}_\sigma}}\tilde{t}_{\sigma\sigma}+\sqrt{\frac{v_\sigma}{\tilde{v}_{-\sigma}}}\tilde{t}_{-\sigma\sigma}, \tag{A1b}$$

$$ik_\sigma(1-\tilde{r}_{\sigma\sigma})=i(\tilde{k}_\sigma-\sigma k_\lambda A_\sigma)\sqrt{\frac{v_\sigma}{\tilde{v}_\sigma}}\tilde{t}_{\sigma\sigma}-(\sigma k_\lambda+\tilde{k}_{-\sigma}A_{-\sigma})\sqrt{\frac{v_\sigma}{\tilde{v}_{-\sigma}}}\tilde{t}_{-\sigma\sigma}, \tag{A1c}$$

$$-ik_{-\sigma}\sqrt{\frac{v_\sigma}{v_{-\sigma}}}\tilde{r}_{-\sigma\sigma}=(\sigma k_\lambda-\tilde{k}_\sigma A_\sigma)\sqrt{\frac{v_\sigma}{\tilde{v}_\sigma}}\tilde{t}_{\sigma\sigma}+i(\tilde{k}_{-\sigma}+\sigma k_\lambda A_{-\sigma})\sqrt{\frac{v_\sigma}{\tilde{v}_{-\sigma}}}\tilde{t}_{-\sigma\sigma}, \tag{A1d}$$

while for $\tilde{r}'^{(\mathrm{L})}_{\sigma' n;\sigma n}$ and $\tilde{t}'^{(\mathrm{L})}_{\sigma' n;\sigma n}$ we have

$$1+\tilde{r}'_{\sigma\sigma}+iA_{-\sigma}\sqrt{\frac{\tilde{v}_\sigma}{\tilde{v}_{-\sigma}}}\tilde{r}'_{-\sigma\sigma}=\sqrt{\frac{\tilde{v}_\sigma}{v_\sigma}}\tilde{t}'_{\sigma\sigma}, \tag{A2a}$$

$$-iA_\sigma(1-\tilde{r}'_{\sigma\sigma})+\sqrt{\frac{\tilde{v}_\sigma}{\tilde{v}_{-\sigma}}}\tilde{r}'_{-\sigma\sigma}=\sqrt{\frac{\tilde{v}_\sigma}{v_{-\sigma}}}\tilde{t}'_{-\sigma\sigma}, \tag{A2b}$$

$$-i(\tilde{k}_\sigma-\sigma k_\lambda A_\sigma)(1-\tilde{r}'_{\sigma\sigma})-(\sigma k_\lambda+\tilde{k}_{-\sigma}A_{-\sigma})\sqrt{\frac{\tilde{v}_\sigma}{v_{-\sigma}}}\tilde{r}'_{-\sigma\sigma}=-ik_\sigma\sqrt{\frac{\tilde{v}_\sigma}{v_\sigma}}\tilde{t}'_{\sigma\sigma}, \tag{A2c}$$

$$(\sigma k_\lambda-\tilde{k}_\sigma A_\sigma)(1+\tilde{r}'_{\sigma\sigma})+i(\tilde{k}_{-\sigma}+\sigma k_\lambda A_{-\sigma})\sqrt{\frac{\tilde{v}_\sigma}{v_{-\sigma}}}\tilde{r}'_{-\sigma\sigma}=-ik_{-\sigma}\sqrt{\frac{\tilde{v}_\sigma}{v_{-\sigma}}}\tilde{t}'_{-\sigma\sigma}. \tag{A2d}$$

We present only the equations for the elements of $\tilde{s}^{(\mathrm{L})}$ explicitly; because of the symmetry of the spiral domain wall profile [Eq. (14)], the elements of $\tilde{s}^{(\mathrm{R})}$ can be found from Eqs. (A1) and (A2) after interchanging $r_{\sigma'\sigma}\leftrightarrow r'_{\sigma'\sigma}$, $t_{\sigma'\sigma}\leftrightarrow t'_{\sigma'\sigma}$ and replacing $k_\lambda\rightarrow -k_\lambda$.

APPENDIX B: DELTA FUNCTION SCATTERING MATRICES IN UNIFORM AND DOMAIN WALL POTENTIALS

We now consider the scattering matrices for a delta function scatterer located in regions of uniform and rotating mag-

netization, $s^{(\delta)}(y_\alpha)$ and $\tilde{s}^{(\delta)}(y_\alpha)$. In the uniform case, $s^{(\delta)}(y_\alpha)$ can be obtained using the result for a spin-independent delta function potential.[26] The individual amplitudes are given by

$$t^{(\delta)}_{\sigma' n';\sigma n} = t'^{(\delta)}_{\sigma' n';\sigma n} = \delta_{\sigma'\sigma}[\mathcal{M}^{-1}_\sigma]_{n'n}, \tag{B1a}$$

$$r^{(\delta)}_{\sigma' n';\sigma n} = r'^{(\delta)}_{\sigma' n';\sigma n} = t^{(\delta)}_{\sigma' n';\sigma n} - \delta_{n'n}, \tag{B1b}$$

where $\mathcal{M}_\sigma$ is an $N_\sigma \times N_\sigma$ matrix with elements

$$[\mathcal{M}_\sigma]_{n'n} = \delta_{n'n} + \frac{iu_\sigma \phi_{n'}(y_\alpha)\phi_n(y_\alpha)}{\hbar\sqrt{v_{\sigma n'} v_{\sigma n}}}. \tag{B2}$$

The scattering matrix for a delta function located inside a domain wall, $\tilde{s}^{(\delta)}(y_\alpha)$, is more complicated because the domain wall basis states $\tilde{\psi}_{\sigma n}(\vec{r})$ couple up and down components. Defining $\beta_n = A_{\sigma n}A_{-\sigma n}$ we have

$$\tilde{t}^{(\delta)}_{\sigma n';\sigma n} = \tilde{t}'^{(\delta)}_{\sigma n';\sigma n} = \sqrt{\frac{\tilde{v}_{\sigma n'}}{\tilde{v}_{\sigma n}}}\frac{1}{1+\beta_{n'}}([\tau_{\sigma\sigma}]_{n'n} - iA_{-\sigma n'}[\tau_{-\sigma\sigma}]_{n'n}), \tag{B3a}$$

$$\tilde{t}^{(\delta)}_{-\sigma n';\sigma n} = -\tilde{t}'^{(\delta)}_{-\sigma n';\sigma n} = \sqrt{\frac{\tilde{v}_{-\sigma n'}}{\tilde{v}_{\sigma n}}}\frac{1}{1+\beta_{n'}}(-iA_{\sigma n'}[\tau_{\sigma\sigma}]_{n'n} + [\tau_{-\sigma\sigma}]_{n'n}), \tag{B3b}$$

$$\tilde{r}^{(\delta)}_{\sigma n';\sigma n} = \tilde{r}'^{(\delta)}_{\sigma n';\sigma n} = \sqrt{\frac{\tilde{v}_{\sigma n'}}{\tilde{v}_{\sigma n}}}\frac{1}{1+\beta_{n'}}([\tau_{\sigma\sigma}]_{n'n} + iA_{-\sigma n'}[\tau_{-\sigma\sigma}]_{n'n} - (1-\beta_{n'})\delta_{n'n}), \tag{B3c}$$

$$\tilde{r}^{(\delta)}_{-\sigma n';\sigma n} = -\tilde{r}'^{(\delta)}_{-\sigma n';\sigma n} = \sqrt{\frac{\tilde{v}_{-\sigma n'}}{\tilde{v}_{\sigma n}}}\frac{1}{1+\beta_{n'}}(iA_{\sigma n'}[\tau_{\sigma\sigma}]_{n'n} + [\tau_{-\sigma\sigma}]_{n'n} - 2iA_{\sigma n'}\delta_{n'n}), \tag{B3d}$$

where $\tau_{\sigma'\sigma}$ and $\tilde{\mathcal{M}}_\sigma$ are matrices of dimension $\tilde{N}_{\sigma'} \times \tilde{N}_\sigma$ and $\tilde{N}_\sigma \times \tilde{N}_\sigma$, respectively, defined by

$$[\tau_{\sigma\sigma}]_{n'n} = [\tilde{\mathcal{M}}^{-1}_\sigma]_{n'n}, \tag{B4a}$$

$$[\tau_{-\sigma\sigma}]_{n'n} = iA_{\sigma n}[\tilde{\mathcal{M}}^{-1}_{-\sigma}]_{n'n}, \tag{B4b}$$

$$[\tilde{\mathcal{M}}_\sigma]_{n'n} = \delta_{n'n} - \frac{mu_\sigma}{i\hbar^2}\frac{(1+\beta_{n'})\phi_{n'}(y_\alpha)\phi_n(y_\alpha)}{\tilde{k}_{\sigma n'} + \beta_{n'}\tilde{k}_{-\sigma n'}}. \tag{B4c}$$

The amplitudes in Eqs. (B1) and (B3) determine the matrices $s^{(\delta)}(y_\alpha)$ and $\tilde{s}^{(\delta)}(y_\alpha)$ that are composed numerically for each impurity configuration in order to obtain the total transmission coefficients in various regimes.

APPENDIX C: DELTA FUNCTION SCATTERING IN WEAK DISORDER LIMIT

In the limit of weak disorder, $u_\sigma \to 0$, transport through the impurity potential $V(\vec{r})$ [Eqs. (22)–(24)] can be treated within the Born approximation. This approach yields the scattering amplitudes to lowest order in u_σ. For the uniformly magnetized case, we have

$$t^{(\mathrm{uni})}_{\sigma' n';\sigma n} = \delta_{\sigma'\sigma}e^{ik_{\sigma' n'}\lambda}\left\{\delta_{n'n} - \frac{iu_\sigma}{\hbar\sqrt{v_{\sigma n'}v_{\sigma n}}} \times \sum_{\alpha=1}^{N_\mathrm{i}} \phi_{n'}(y_\alpha)\phi_n(y_\alpha)e^{i(k_{\sigma n}-k_{\sigma n'})z_\alpha}\right\} + O(u_\sigma^2), \tag{C1a}$$

$$r^{(\mathrm{uni})}_{\sigma' n';\sigma n} = -\delta_{\sigma'\sigma}\frac{iu_\sigma}{\hbar\sqrt{v_{\sigma n'}v_{\sigma n}}}\sum_{\alpha=1}^{N_\mathrm{i}} \phi_{n'}(y_\alpha)\phi_n(y_\alpha)e^{i(k_{\sigma n'}+k_{\sigma n})z_\alpha} + O(u_\sigma^2). \tag{C1b}$$

In the case of a domain wall, the situation is more complicated because scattering from the interfaces at $z=0,\lambda$ leads to mixing of up and down spin channels. It is most convenient to first calculate amplitudes for transport through the disordered region $0<z<\lambda$, not including the interfaces, which we write $\tilde{t}^{(N_\mathrm{i}\times\delta)}_{\sigma' n';\sigma n}$ and $\tilde{r}^{(N_\mathrm{i}\times\delta)}_{\sigma' n';\sigma n}$. Formally, these coefficients correspond to a scenario in which the rotating potential $\theta(z)=\pi z/\lambda$ is valid for *all* z, so that the asymptotic states are the domain wall basis states $\tilde{\psi}^{\gtrless}_{\sigma n}(\vec{r})$. Within the Born approximation, these amplitudes are given by

$$\tilde{t}^{(N_\mathrm{i}\times\delta)}_{\sigma n';\sigma n} = e^{i\tilde{k}_{\sigma n'}\lambda}\left\{\delta_{n'n} - \frac{i(u_\sigma + u_{-\sigma}A_{\sigma n'}A_{\sigma n})}{\hbar\sqrt{\tilde{v}_{\sigma n'}\tilde{v}_{\sigma n}}}\sum_{\alpha=1}^{N_\mathrm{i}} \phi_{n'}(y_\alpha)\phi_n(y_\alpha)e^{i(\tilde{k}_{\sigma n}-\tilde{k}_{\sigma n'})z_\alpha}\right\} + O(u_\sigma^2), \tag{C2a}$$

$$\tilde{t}^{(N_\mathrm{i}\times\delta)}_{-\sigma n';\sigma n} = e^{i\tilde{k}_{-\sigma n'}\lambda}\frac{u_{-\sigma}A_{\sigma n} - u_\sigma A_{-\sigma n'}}{\hbar\sqrt{\tilde{v}_{-\sigma n'}\tilde{v}_{\sigma n}}}\sum_{\alpha=1}^{N_\mathrm{i}} \phi_{n'}(y_\alpha)\phi_n(y_\alpha)e^{i(\tilde{k}_{\sigma n}-\tilde{k}_{-\sigma n'})z_\alpha} + O(u_\sigma^2), \tag{C2b}$$

$$\tilde{r}^{(N_\mathrm{i}\times\delta)}_{\sigma n';\sigma n} = -\frac{i(u_\sigma - u_{-\sigma}A_{\sigma n'}A_{\sigma n})}{\hbar\sqrt{\tilde{v}_{\sigma n'}\tilde{v}_{\sigma n}}}\sum_{\alpha=1}^{N_\mathrm{i}} \phi_{n'}(y_\alpha)\phi_n(y_\alpha)e^{i(\tilde{k}_{\sigma n}+\tilde{k}_{\sigma n'})z_\alpha} + O(u_\sigma^2), \tag{C2c}$$

$$\tilde{r}^{(N_i\times\delta)}_{-\sigma n';\sigma n} = \frac{u_{-\sigma}A_{\sigma n} + u_{\sigma}A_{-\sigma n'}}{\hbar\sqrt{\tilde{v}_{\sigma n'}\tilde{v}_{\sigma n}}} \sum_{\alpha=1}^{N_i} \phi_{n'}(y_\alpha)\phi_n(y_\alpha)e^{i(\tilde{k}_{\sigma n}+\tilde{k}_{-\sigma n'})z_\alpha} + O(u_\sigma^2). \tag{C2d}$$

To calculate the *average* scattering probabilities, it is necessary to take the squared magnitude of the quantities in Eqs. (C1) and (C2) and then average over the impurity positions $\vec{r}_\alpha$. Because the positions of different impurities are uncorrelated, the average of terms involving two different impurities are a factor $1/k_F L_z$ smaller than those involving a single impurity. They are therefore negligible, and the scattering is dominated by the single impurity scattering events.[51]

We note that the probabilities corresponding to the amplitudes $t^{(\mathrm{uni})}_{\sigma n;\sigma n}$ and $\tilde{t}^{(N_i\times\delta)}_{\sigma n;\sigma n}$, which are equal to unity in the limit $u_\sigma=0$, cannot be calculated by simply taking the absolute square of the amplitudes in Eqs. (C1a) and (C2a). This is due to the presence of the factor $\delta_{n'n}$, which means that the term of $O(u_\sigma^2)$ in the amplitude [not given in Eqs. (C1a) and (C2a)] also contributes a term of $O(u_\sigma^2)$ in the corresponding probability. It is therefore necessary either to calculate the amplitudes to $O(u_\sigma^2)$ or, more conveniently, to use conservation of probability to express it in terms of the other probabilities.

With these considerations, we find the average probabilities in the uniform case as follows:

$$\langle R^{(\mathrm{uni})}_{\sigma n';\sigma n}\rangle = n_i u_\sigma^2 \frac{L_z}{L_y}\frac{\left(1+\frac{1}{2}\delta_{n'n}\right)}{\hbar^2 v_{\sigma n'}v_{\sigma n}}, \tag{C3a}$$

$$\langle T^{(\mathrm{uni})}_{\sigma n';\sigma n}\rangle = \langle R^{(\mathrm{uni})}_{\sigma n';\sigma n}\rangle, \quad n'\neq n, \tag{C3b}$$

$$\langle T^{(\mathrm{uni})}_{\sigma n;\sigma n}\rangle = 1 - n_i u_\sigma^2 \frac{L_z}{L_y}\sum_{n'=1}^{N_\sigma}\frac{2-\frac{1}{2}\delta_{n'n}}{\hbar^2 v_{\sigma n'}v_{\sigma n}}. \tag{C3c}$$

Summing over all n and n', we can express the total spin-dependent transmission and reflection in terms of the mean free path l_σ [Eq. (27)]:

$$\langle R^{(\mathrm{uni})}_{\sigma'\sigma}\rangle = \delta_{\sigma'\sigma}\frac{\pi}{2}\frac{N_\sigma L_z}{l_\sigma}F_1(N_\sigma), \tag{C4a}$$

$$\langle T^{(\mathrm{uni})}_{\sigma'\sigma}\rangle = N_\sigma - \langle R^{(\mathrm{uni})}_{\sigma'\sigma}\rangle, \tag{C4b}$$

where

$$F_1(N_\sigma) = \frac{k_{\sigma,F}L_y}{\pi N_\sigma}\left(\frac{2}{L_y}\right)^2 \sum_{n'=1}^{N_\sigma}\sum_{n=1}^{N_\sigma}\frac{1+\frac{1}{2}\delta_{n'n}}{k_{\sigma n}k_{\sigma n'}}. \tag{C5}$$

Here $F_1(N_\sigma)$ is a form factor which takes account of the finite number of channels and reduces to unity in the limit $N_\sigma\to\infty$.

In the domain wall case, the probabilities corresponding to the amplitudes in Eqs. (C2) are given by

$$\langle \tilde{R}^{(N_i\times\delta)}_{\sigma n';\sigma n}\rangle = \frac{n_i L_z}{L_y}\frac{1+\frac{1}{2}\delta_{n'n}}{\hbar^2\tilde{v}_{\sigma n'}\tilde{v}_{\sigma n}}(u_\sigma - u_{-\sigma}A_{\sigma n'}A_{\sigma n})^2, \tag{C6a}$$

$$\langle \tilde{R}^{(N_i\times\delta)}_{-\sigma n';\sigma n}\rangle = \frac{n_i L_z}{L_y}\frac{1+\frac{1}{2}\delta_{n'n}}{\hbar^2\tilde{v}_{-\sigma n'}\tilde{v}_{\sigma n}}(u_{-\sigma}A_{\sigma n} + u_\sigma A_{-\sigma n'})^2, \tag{C6b}$$

$$\langle \tilde{T}^{(N_i\times\delta)}_{\sigma n';\sigma n}\rangle = \frac{n_i L_z}{L_y}\frac{1+\frac{1}{2}\delta_{n'n}}{\hbar^2\tilde{v}_{\sigma n'}\tilde{v}_{\sigma n}}(u_\sigma + u_{-\sigma}A_{\sigma n'}A_{\sigma n})^2, \quad n'\neq n, \tag{C6c}$$

$$\langle \tilde{T}^{(N_i\times\delta)}_{-\sigma n';\sigma n}\rangle = \frac{n_i L_z}{L_y}\frac{1+\frac{1}{2}\delta_{n'n}}{\hbar^2\tilde{v}_{-\sigma n'}\tilde{v}_{\sigma n}}(u_{-\sigma}A_{\sigma n} - u_\sigma A_{-\sigma n'})^2, \tag{C6d}$$

$$\langle \tilde{T}^{(N_i\times\delta)}_{\sigma n;\sigma n}\rangle = 1 - \langle \tilde{R}^{(N_i\times\delta)}_{\sigma n;\sigma n}\rangle - \sum_{\substack{n'=1,\\ n'\neq n}}^{\tilde{N}_\sigma}[\langle \tilde{R}^{(N_i\times\delta)}_{\sigma n';\sigma n}\rangle + \langle \tilde{T}^{(N_i\times\delta)}_{\sigma n';\sigma n}\rangle] - \sum_{n'=1}^{\tilde{N}_{-\sigma}}[\langle \tilde{R}^{(N_i\times\delta)}_{-\sigma n';\sigma n}\rangle + \langle \tilde{T}^{(N_i\times\delta)}_{-\sigma n';\sigma n}\rangle]. \tag{C6e}$$

In general, it is nontrivial to incorporate the interfaces and thus obtain the total transmission probabilities for the domain wall, since if there is nonzero reflection from the interfaces then multiple paths through the disordered region need to be considered. The situation simplifies somewhat in the wide wall limit of Eqs. (20), since to $O(1/p_F^2)$ the interface reflection probabilities are zero. The transmission through the entire domain wall, including both interfaces and the disordered region, can then be found by multiplying the transmission of each part. Furthermore, since the interface transmission is diagonal in transverse channel number, only intermediate spin states need to be summed over.

It is simplest to consider the incoherent case, since the probabilities are taken before combining with the interfaces, meaning that the results of Eqs. (C3)–(C6) can be used directly. In particular, for the transmission and reflection probabilities from the left we have

$$\langle \tilde{T}^{(\mathrm{dw})}_{\sigma' n';\sigma n} \rangle = \sum_{\sigma_1,\sigma_2=\pm} \tilde{T}^{(\mathrm{R})}_{\sigma' n';\sigma_1 n'} \langle \tilde{T}^{(N_i\times\delta)}_{\sigma_1 n';\sigma_2 n} \rangle \tilde{T}^{(\mathrm{L})}_{\sigma_2 n;\sigma n}, \quad \text{(C7a)}$$

$$\langle \tilde{R}^{(\mathrm{dw})}_{\sigma' n';\sigma n} \rangle = \sum_{\sigma_1,\sigma_2=\pm} \tilde{T}'^{(\mathrm{L})}_{\sigma' n';\sigma_1 n'} \langle \tilde{R}^{(N_i\times\delta)}_{\sigma_1 n';\sigma_2 n} \rangle \tilde{T}^{(\mathrm{L})}_{\sigma_2 n;\sigma n}. \quad \text{(C7b)}$$

The total spin-dependent probabilities, $\langle \tilde{T}^{(\mathrm{dw})}_{\sigma'\sigma} \rangle$ and $\langle \tilde{R}^{(\mathrm{dw})}_{\sigma'\sigma} \rangle$, may be found by summing over the previous expressions, yielding quite cumbersome expressions. Of particular interest, however, is the transmission with spin-mistracking, $\langle \tilde{T}^{(\mathrm{dw})}_{-\sigma\sigma} \rangle$, which is given by

$$\langle \tilde{T}^{(\mathrm{dw})}_{-\sigma\sigma} \rangle = \frac{2N_\sigma}{3p_\mathrm{F}^2}\left\{ F_2(N_\sigma) - \frac{6}{\pi}\frac{L_z}{l_+}\frac{N_\sigma}{k_\mathrm{F}L_y/\pi}\left[\rho + \frac{\pi^2}{8}(1+\rho^2)F_3(N_\sigma) + \frac{(1+\rho)^2}{8N_\sigma} \right] \right\}, \quad \text{(C8)}$$

where

$$F_2(N_\sigma) = \frac{3}{2}\left[1 - \left(\frac{\pi}{k_\mathrm{F}L_y}\right)^2 \frac{(N_\sigma+1)(2N_\sigma+1)}{6} \right], \quad \text{(C9)}$$

$$F_3(N_\sigma) = \frac{8}{N_\sigma^2\pi^2}\sum_{n'=1}^{N_\sigma}\sum_{n=1}^{N_\sigma}\frac{k_{0n}}{k_{0n'}}. \quad \text{(C10)}$$

Here $F_2(N_\sigma)$ and $F_3(N_\sigma)$ are form factors which reduce to unity in the limit $L_y \to \infty$. Note that in the approximation used here we have $k_{+,\mathrm{F}}=k_{-,\mathrm{F}}=k_\mathrm{F}$ and $N_+=N_-$. Equation (C8) shows that the initial slope of $\tilde{T}^{(\mathrm{dw})}_{-\sigma\sigma}$ as a function of $1/l_+$ is *always negative*, which explains the observed behavior in the inset of Fig. 4.

Another important insight permitted by the perturbative approach is the spin-dependent difference in transmission $\Delta T_\pm$. Here we find

$$\langle \Delta T_\sigma \rangle = -\sigma\frac{4}{\pi}\frac{\rho-1}{p_\mathrm{F}^2}\frac{N_\sigma L_z}{l_+}\left(\frac{N_\sigma\pi}{k_\mathrm{F}L_y}\right)\left\{ \frac{\pi^2}{8}F_3(N_\sigma) + \frac{1}{2N_\sigma} \right\}. \quad \text{(C11)}$$

Equation (C11) shows that $\langle \Delta T_\sigma \rangle$ increases linearly with $1/l_+$ for weak disorder, with a slope whose sign depends on σ. This explains the behavior of $\langle \Delta T_\sigma \rangle$ observed in Fig. 5(b).

Interestingly, the sum $\langle \Delta T_+ \rangle + \langle \Delta T_- \rangle$ in Eq. (C11) is zero, implying that the intrinsic magnetoconductance $\langle \Delta g \rangle$ is zero to first order in $1/l_+$. This is in agreement with our numerical results for $\langle \Delta g \rangle$, which show a quadratic dependence on $1/l_+$ for small disorder.

Finally, we point out that for spin-independent disorder, $\rho=1$, Eq. (C11) predicts that $\langle \Delta T_\sigma \rangle = 0$. This is because in this case, the only spin-dependence of scattering comes from the difference in the up and down wave vectors, which are treated as zero in the approximation of Eqs. (20).

APPENDIX D: SPIN-MIXING IN A ONE-DIMENSIONAL MODEL

The results of Sec. III A for the transmission and reflection through a sequence of impurity scatterings show that repeated scattering from delta functions in a domain wall leads to a relative increase of the spin-mixing transmission and reflection coefficients, $T_{-\sigma\sigma}$ and $R_{-\sigma\sigma}$. We now gain some insight into this mechanism through a simple toy model which captures some essential features of the problem. In particular, consider a one-dimensional sequence of idealized spin-mixing scatterers for which there is zero reflection and for which the spin-dependent transmission probabilities are

$$T = T' = \begin{pmatrix} 1-\epsilon_+ & \epsilon_- \\ \epsilon_+ & 1-\epsilon_- \end{pmatrix}. \quad \text{(D1)}$$

Here $\epsilon_\pm$ represent the off-diagonal scattering. Technically, this model is actually an example of a *Markov chain*, widely studied in probability theory.[52]

The absence of reflection allows us to calculate the total transmission through N_i scatterers by taking T^{N_i}. Diagonalizing T and taking powers of the diagonal components, we evaluate this as

$$T^{N_\mathrm{i}} = \frac{1}{\epsilon_+ + \epsilon_-}\begin{pmatrix} \epsilon_- + \epsilon_+\chi^{N_\mathrm{i}} & \epsilon_-(1-\chi^{N_\mathrm{i}}) \\ \epsilon_+(1-\chi^{N_\mathrm{i}}) & \epsilon_+ + \epsilon_-\chi^{N_\mathrm{i}} \end{pmatrix}, \quad \text{(D2)}$$

where $\chi = 1-\epsilon_+-\epsilon_-$. In the limit of infinitely many scatterers this reduces to

$$T^\infty = \frac{1}{\epsilon_+ + \epsilon_-}\begin{pmatrix} \epsilon_- & \epsilon_- \\ \epsilon_+ & \epsilon_+ \end{pmatrix}. \quad \text{(D3)}$$

We thus observe that the spin-flip scattering, when accumulated over many events, leads to a complete mixing of spin, with the relative weightings determined by $\epsilon_\sigma/(\epsilon_+ + \epsilon_-)$. In the special case of spin-independent scattering, $\epsilon_+ = \epsilon_-$, all matrix elements in the rhs of Eq. (D3) are equal and hence, for a given incoming spin direction, the transmission is mixed equally between both spin directions.

The transmission T^∞ reproduces qualitatively the behavior of the *fractional* transmission from Sec. III A, i.e., $T_{\sigma'\sigma}/(T_{\sigma\sigma}+T_{-\sigma\sigma})$. Obviously, such a simplified picture does not reproduce the actual results on a quantitative level. However, the qualitative resemblance suggests that it captures an essential feature of transmission through a disordered domain wall, namely, a spin-mixing effect which accumulates (and saturates) over successive scattering events.

*Electronic address: jalabert@ipcms.u-strasbg.fr

[1] U. Ruediger, J. Yu, S. Zhang, A. D. Kent, and S. S. P. Parkin, Phys. Rev. Lett. **80**, 5639 (1998).

[2] K. Hong and N. Giordano, J. Phys.: Condens. Matter **10**, L401 (1998).

[3] U. Rüdiger, J. Yu, L. Thomas, S. S. P. Parkin, and A. D. Kent, Phys. Rev. B **59**, 11914 (1999).

[4] U. Ebels, A. Radulescu, Y. Henry, L. Piraux, and K. Ounadjela, Phys. Rev. Lett. **84**, 983 (2000).

[5] G. Dumpich, T. P. Krome, and B. Hausmanns, J. Magn. Magn. Mater. **248**, 241 (2002).

[6] J. B. A. N. van Hoof, K. M. Schep, A. Brataas, G. E. W. Bauer, and P. J. Kelly, Phys. Rev. B **59**, 138 (1999).

[7] J. Kudrnovský, V. Drchal, I. Turek, P. Středa, and P. Bruno, Surf. Sci. **482–485**, 1107 (2001).

[8] N. F. Mott, Proc. R. Soc. London, Ser. A **153**, 699 (1936).

[9] G. G. Cabrera and L. M. Falicov, Phys. Status Solidi B **61**, 539 (1974).

[10] D. Weinmann, R. L. Stamps, and R. A. Jalabert, in *Electronic Correlations: From Meso- to Nano-physics*, edited by T. Martin, G. Montambaux, and J. Trân Thanh Vân (EDP Sciences, Les Ulis, 2001).

[11] H. Imamura, N. Kobayashi, S. Takahashi, and S. Maekawa, Phys. Rev. Lett. **84**, 1003 (2000).

[12] K. Nakanishi and Y. O. Nakamura, Phys. Rev. B **61**, 11278 (2000).

[13] V. K. Dugaev, J. Berakdar, and J. Barnaś, Phys. Rev. B **68**, 104434 (2003).

[14] M. Viret, D. Vignoles, D. Cole, J. M. D. Coey, W. Allen, D. S. Daniel, and J. F. Gregg, Phys. Rev. B **53**, 8464 (1996).

[15] V. A. Gopar, D. Weinmann, R. A. Jalabert, and R. L. Stamps, Phys. Rev. B **69**, 014426 (2004).

[16] P. E. Falloon, R. A. Jalabert, D. Weinmann, and R. L. Stamps, Phys. Rev. B **70**, 174424 (2004).

[17] T. Valet and A. Fert, Phys. Rev. B **48**, 7099 (1993).

[18] P. M. Levy and S. Zhang, Phys. Rev. Lett. **79**, 5110 (1997).

[19] A. Brataas, G. Tatara, and G. E. W. Bauer, Phys. Rev. B **60**, 3406 (1999).

[20] G. Tatara and H. Fukuyama, Phys. Rev. Lett. **78**, 3773 (1997).

[21] Y. Lyanda-Geller, I. L. Aleiner, and P. M. Goldbart, Phys. Rev. Lett. **81**, 3215 (1998).

[22] P. A. E. Jonkers, S. J. Pickering, H. De Raedt, and G. Tatara, Phys. Rev. B **60**, 15970 (1999).

[23] E. P. Wohlfarth, in *Ferromagnetic Materials*, edited by E. P. Wohlfarth (North-Holland, Amsterdam, 1982), Vol. 1, pp. 1–70.

[24] M. Getzlaff, J. Bansmann, J. Braun, and G. Schönhense, J. Magn. Magn. Mater. **161**, 70 (1996).

[25] M. Büttiker, Y. Imry, R. Landauer, and S. Pinhas, Phys. Rev. B **31**, 6207 (1985).

[26] M. Cahay, M. McLennan, and S. Datta, Phys. Rev. B **37**, 10125 (1988).

[27] C. W. J. Beenakker, Rev. Mod. Phys. **69**, 731 (1997).

[28] P. A. Mello and S. Tomsovic, Phys. Rev. B **46**, 15963 (1992).

[29] A. D. Stone, P. A. Mello, K. A. Muttalib, and J.-L. Pichard, in *Mesoscopic Phenomena in Solids*, edited by B. L. Altshuler, P. A. Lee, and R. A. Webb (Elsevier Science, New York, 1991), Chap. 9, pp. 369–448.

[30] D. Frustaglia, M. Hentschel, and K. Richter, Phys. Rev. Lett. **87**, 256602 (2001).

[31] G. Bergmann, Phys. Rep. **107**, 1 (1984).

[32] B. Kramer and A. MacKinnon, Rep. Prog. Phys. **56**, 1469 (1993).

[33] L. Schiff, *Quantum Mechanics*, 3rd ed. (McGraw-Hill, New York, 1968).

[34] X. Waintal and M. Viret, Europhys. Lett. **65**, 427 (2004).

[35] S. Datta, *Electron Transport in Mesoscopic Systems* (Cambridge University Press, Cambridge, England, 1997).

[36] I. Petej and J. F. Gregg, in *Magnetism: Molecules to Materials III*, edited by J. S. Miller and M. Drillon (Wiley-VCH, Weinheim, 2002), pp. 253–296.

[37] A. D. Stone, in *Physics of Nanostructures*, edited by J. H. Davies and A. R. Long (IOP, Bristol, 1992), pp. 65–100.

[38] For a single delta function, $\langle R_{\sigma\sigma'}^{(\delta)} \rangle$ can be found from Eq. (C4a) after setting $N_i=1$ and $n_i=1/L_yL_z$.

[39] This can be understood intuitively by considering the delta function as an obstacle in real space. Since the delta function is narrower than a transverse channel in real-space (whose width is on the order of $1/k_F$), the maximum reflection corresponds to one channel being completely blocked.

[40] P. A. Mello and A. D. Stone, Phys. Rev. B **44**, 3559 (1991).

[41] M. J. M. de Jong, Phys. Rev. B **49**, 7778 (1994).

[42] K. Richter, D. Ullmo, and R. A. Jalabert, J. Math. Phys. **37**, 5087 (1996).

[43] H. U. Baranger, Phys. Rev. B **42**, 11479 (1990).

[44] M. Popp, D. Frustaglia, and K. Richter, Phys. Rev. B **68**, 041303(R) (2003).

[45] G. Tatara, Int. J. Mod. Phys. B **15**, 321 (2001).

[46] In the limit $\lambda \to \infty$, the domain wall becomes perfectly adiabatic and $\langle \Delta g_{co} \rangle$ should go to zero. However, for the system sizes we are able to treat numerically, this limit corresponds to values of λ much larger than the localization length $(N_\sigma l_\sigma)$, for which the system is in the strongly localized regime and is therefore not relevant for diffusive transport.

[47] P. A. Lee and A. D. Stone, Phys. Rev. Lett. **55**, 1622 (1985).

[48] P. E. Falloon, Ph.D. thesis, University of Western Australia-Université Louis Pasteur (2006), URL:http://eprints-scd-ulp.u-strasbg.fr:8080/553/

[49] The necessary condition for complex $\tilde{k}_{\sigma n}$ is that $k_{\sigma n}$ is real [so that the (σ,n) channel is open] while k_{0n} is imaginary, such that the term inside the second square root in Eq. (18a) is negative. This can only occur if $k_\Delta < \sqrt{8} k_\lambda$, which corresponds to a wall width narrower than a single Larmor precession length and is therefore not applicable for the systems we are considering in this paper.

[50] D. Chiba, M. Yamanouchi, F. Matsukura, T. Dietl, and H. Ohno, Phys. Rev. Lett. **96**, 096602 (2006).

[51] R. A. Jalabert and J.-L. Pichard, J. Phys. I **5**, 287 (1995).

[52] G. R. Grimmett and D. R. Stirzaker, *Probability and Random Processes*, 3rd ed. (Oxford University Press, Oxford, 2004).